MASTER THESIS

To obtain the Master degree by Politecnico of Turin

STUDY OF THE DEPOSITION OF DOPED COPPER(I) OXIDE BY "AA-MOCVD" AS P-TYPE TRANSPARENT CONDUCTING MATERIAL

Prepared by:

Lorenzo Bottiglieri

student n°: 242106

Supervised by:

Doctor Stefano Bianco

Doctor Jean-Luc Deschanvres,

Doctor Maria del Carmen Jimenez Arevalo

Co-supervised by: Doctor Joao Avelas Resend

at: Laboratoire des Materiaux et du genie Physique (LMGP)

“A poet once said, 'The whole universe is in a glass of wine.' We will probably never know in what sense he meant it, for poets do not write to be understood. But it is true that if we look at a glass of wine closely enough we see the entire universe. There are the things of physics: the twisting liquid which evaporates depending on the wind and weather, the reflection in the glass; and our imagination adds atoms. The glass is a distillation of the earth's rocks, and in its composition we see the secrets of the universe's age, and the evolution of stars. What strange array of chemicals are in the wine? How did they come to be? There are the ferments, the enzymes, the substrates, and the products. There in wine is found the great generalization; all life is fermentation. Nobody can discover the chemistry of wine without discovering, as did Louis Pasteur, the cause of much disease. How vivid is the claret, pressing its existence into the consciousness that watches it! If our small minds, for some convenience, divide this glass of wine, this universe, into parts -- physics, biology, geology, astronomy, psychology, and so on -- remember that nature does not know it! So let us put it all back together, not forgetting ultimately what it is for. Let it give us one more final pleasure; drink it and forget it all!”
— Richard P. Feynman

Acknowledgment

Firstly, I would like to acknowledge my master thesis reference professor Dr. Stefano Bianco of the DISAT at the Politecnico of Torino as the main reader of this thesis, I am gratefully indebted to his advices and for his very valuable comments on this thesis and I am very thankful for the time he dedicated to me and his very important help.

I would like to thank my supervisor of the laboratory LMGP Dr. Jean-Luc Deschanvres. The door of the Dr. Deschanvres' office was always open whenever I ran into a trouble spot or had a question about my research or writing. Moreover, I would like to thank another fundamental person for the writing of this master thesis, Dr. Joao Avelas Resende of the laboratory LMGP, who always help me during the experiments, explaining to me all the procedures and strongly assist me during the writing of this work.

I would also like to thank the expert who was involved in this research project, Dr. Maria del Carmen Jimenez Arevalo of the laboratory LMGP, whose support and advices were very useful during this experience.

Finally, I must express my very profound gratitude to my parents, to my brother and to my friends for providing me with unfailing support and continuous encouragement throughout my years of study and through the process of researching and writing this thesis. This accomplishment would not have been possible without them.

Thank you.

Lorenzo Bottiglieri.

1. TRANSPARENT ELECTRONICS & COPPER OXIDE 7

1.1 Transparent electronics and Transparent Conductive Oxides (TCOs) 7
1.2 Cuprous oxide Cu_2O 9
1.3 Conduction in Cu_2O 10
1.4 Copper oxide doping systems 11

2. EXPERIMENTAL SETUP AND CHARACTERIZATION PROCEDURE 14

2.1 Aerosol-Assisted Metal Organic Chemical Vapour Deposition 14
2.2 Deposition experimental description 16
2.3 Characterization techniques 18
2.4 4-probe measurement 19
2.5 Optical transmittance 19
2.6 X-ray photoelectron spectroscopy (XPS) 20
2.7 Scanning Electron Microscopy (SEM) & Energy Dispersive Spectroscopy (EDS) 20
2.8 Raman spectroscopy 21
2.9 Thermal Annealing 22

3. PURE COPPER OXIDE DEPOSITION 23

3.1 Structural properties 23
3.2 Morphological characteristics 25
3.3 Electrical properties 26
3.4 Optical properties 28
3.5 Thermal treatment 30

4. TIN DOPED CUPROUS OXIDE (SN/SN+CU) 33

4.1 Effect on the different tin precursors 34
4.1.1 Structural properties 34
4.1.2 Morphological characteristics 36
4.1.3 Electrical properties 38
4.1.4 Optical properties 39
4.1.5 Thermal treatment 41
4.2 Tin doped copper oxide results with Dibutyltin Diacetate as Precursor 43
4.2.1 Structural properties 43
4.2.2 Morphological characteristics 44
4.2.3 Electrical properties 48
4.2.4 Optical properties 48

4.2.5 Thermal treatment 50

5. LITHIUM DOPED CUPROUS OXIDE (LI/LI+CU) 53

LITHIUM DOPED AND PRECURSOR 53

5.1 STRUCTURAL PROPERTIES 54

5.2 MORPHOLOGICAL CHARACTERISTICS 55

5.3 ELECTRICAL PROPERTIES 57

5.4 OPTICAL PROPERTIES 58

CONCLUSIONS 61

Preface

This master thesis is focused on the study of the deposition by Aerosol Assisted Metal Organic Chemical Vapor Deposition (AA-MOCVD) of doped copper(I) oxide, Cu_2O, thin films. Among the semiconducting compounds, copper oxides present the most promising electrical, optical and productive features that establish these materials suitable as p-type semiconductors. This research will be aimed on the optimization of the deposition of pure and doped-copper oxide.

In the first chapter, there will be an overlook of transparent conductive materials and of the so called transparent electronics, it will contain also a summary of the physical properties of the Cuprous oxide, how conduction takes place in this material and there will be a special focus on the already existing doped copper oxide systems and their possible applications.

In the chapter II there will be the description of the AAMOCVD system and the experimental setup followed by a complete explanation on how deposition occurs. Moreover, the used characterization tools will be described and how these systems work.

The third chapter is dedicated to the explanation of the pure copper oxide deposition and its optimization and then the analysis of the results for these depositions.

In the work on Cu_2O, different depositions took place to establish the optimized deposition condition trying to get the best film in terms of conductivity and optical transmittance. Once obtained the best deposition conditions, there is a focus on the depositions of doped Cu_2O, with the purpose to enhance the electrical and optical properties of the films.

The 4^{th} chapter will be dedicated to the study of the effect of the Tin as dopant on the copper oxide deposition. This chapter will be divided in two sections. The first study aims to test and to investigate the incorporation of Tin in the film through the use of different chemical precursors starting from the obtained results from DBTD.

The second section will be related to the effect of the precursor already studied in Resende[1], the Dibutyltin Diacetate (DBTD) as precursor for the Tin doping and how the doping level influences the performance of the film.

The study of Lithium doped copper oxide phase CuLiO is described in the chapter V, discussing the results obtained with this dopant through the analysis of the produced films using the characterization tools described in chapter II, investigating the main parameters in terms of electrical and optical properties.

For each chapter, the results will be presented divided between structural, morphological then electrical and optical properties of the as deposited samples. Moreover, every chapter will contain also the annealing studies performed on the samples.

1. Transparent Electronics & copper oxide

1.1 Transparent electronics and Transparent Conductive Oxides (TCOs)

Transparent electronic is the research field where the classical opaque semiconductor materials are replaced by the use of transparent ones, which should be characterized by a high electrical conductivity and especially by an elevated optical transmittance.

This requires a special class of materials because, from the bands diagram point of view, the combination of transparency and conductivity is contradictory. In fact, a material which is transparent in the visible range (390nm-700nm) has a large energy gap and this implies a limited electrical conduction.

In literature many materials with the required properties are been reported, among them oxides, transparent conductive oxide (TCOs') are the most widely used. These developed materials are characterized by the fact that the conduction take place in conduction band i.e. they are n-type materials, but there is still a lack of p-type TCO. For this reason, this research is focused on the growth of a p-type transparent conductive oxide.

These oxides has been studied for the possibility to exploit theirs properties in many different applications such as sensor[2–6], gas sensor[7], solar panel[6–11], screens [12,13] and electrodes[12,14,15]. Moreover, many research groups are focusing their attention on the possibility to create light control windows, light emitting diode[9,13,16] and also light absorber[16–18].

The reduced size due to the possibility of such material to be deposited in thin film leads the possibility to developed Thin Film Transistor(TFT)[19,20] also used in Liquid Cristal Display (LCD)[21]. Furthermore, the properties of transparency and conductivity lead the creation of Transparent TFT (TTFT)[22] that will be the starting point for the transparent electronic, i.e. circuit able to perform computational operations letting the light pass through. This kind of technology can be integrated in flexible substrate[13,23] leading the possibility to highly increase the application they can be used for. This is one of the main advantages of this class of materials and this would lead to the development of very wide range applications as for graphene oxides shown in Wang[24].

The key parameter to achieve both optical transparency and electrical conductivity in TCO's is the energy gap. To overcome the band gap, electrical conductivity in TCOs is achieved by increasing the number of free charge carriers through intrinsic defects, such as oxygen vacancies, or through extrinsic dopants, typically metal cations with an extra charge so a higher valence.

In n-type semiconductors, these dopants or defects provide energy levels close to the bottom of the conduction band, allowing those electrons to be promoted into the conduction band as free charge carriers. In p-type semiconductors, the additional energy levels are close to the top of the

valence band, allowing electrons to be promoted into the extra energy levels and creating holes in the valence band, which will act as free charge carriers.

Among the already developed TCO[25] semiconductors the most important are ZnO[16,26], In_2O_3[9,25] and SnO_2[22,27], as well as the ternary compounds Zn_2SnO_4, $ZnSnO_3$, $Zn_3In_2O_6$, In_2SnO_4, $CdSnO_3$. Moreover, multi-component oxides consisting of combinations of ZnO[16,28] and SnO_2 and Sn doped In_2O_3 (ITO)[12,29,30] were created and studied. The latter compound is the widest used since for good performances but shows economical disadvantages due to the high cost of indium and its low disposability[31], for these reasons many groups are working in find a substitute of this material with the same performances as shown in Minami[21].

From the p-type transparent conductive oxide's point of view, instead, many research groups reported different types of materials such as NiO[32], Cu:NiO[33], Cu_2O[1,34], $CuScO_2$[35], $CuAlS_2$[36], but the performances of this class of oxides are not suitable for applications. For this reason, many research groups are working on the possibility to develop and grow materials that have both the required properties, i.e. a good electrical conduction and transparency.
In figure 1.1, some of the already developed TCO and some of their applications is shown.

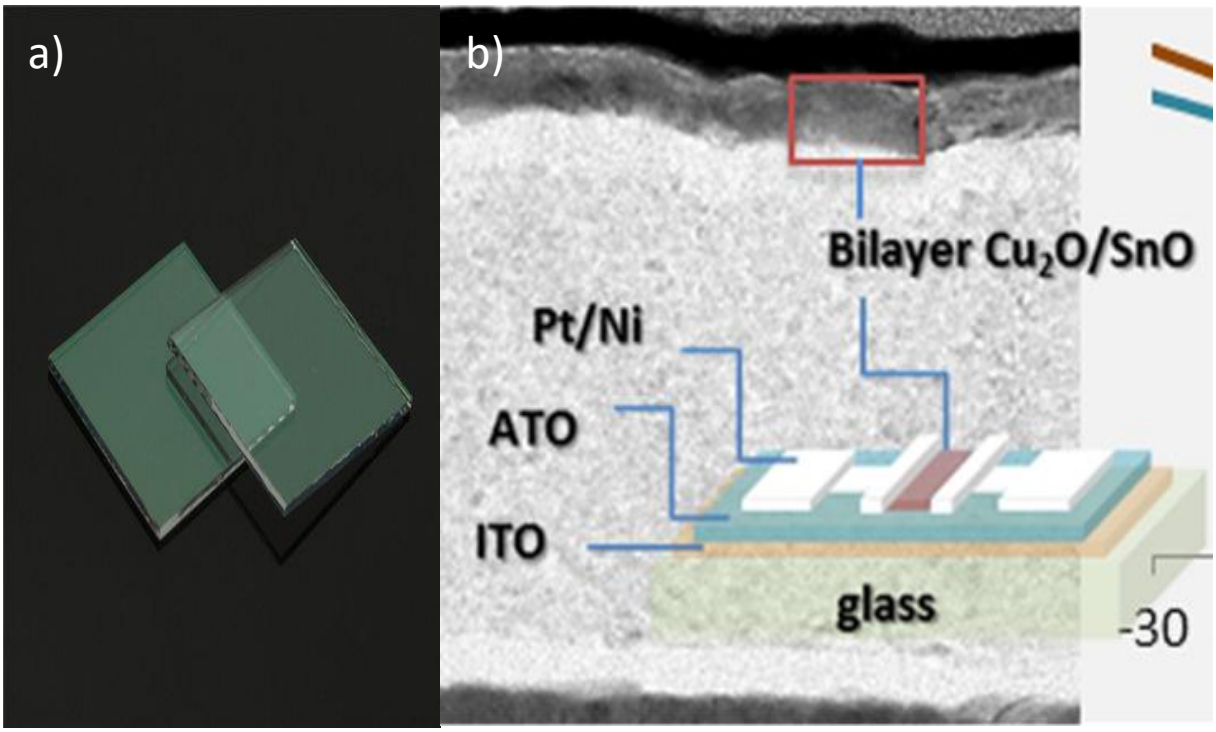

Figure 1.1 a)Indium Tin Oxide (ITO) conductive glass producted by Sabdel b) bylayer TFT with p-type Cu2O and SnO channel obtained by Hala A. Al-Jawhari[112]

1.2 Cuprous oxide Cu_2O

The increasing interest of the scientific community in the TCO technology and the lack of a p-type material with the required properties is been the starting point for many researchers' groups to investigate the growth and the deposition of new materials. Among the many possibilities, one the promising materials is the cuprous oxide, Cu_2O, because of its possible feature as p-type semiconductor which belongs the required properties and it is nontoxic and abundant.

From the crystallographic point of view, the cuprous oxide has a cubic crystalline structure with lattice parameter of 4.2696 Å. The Cu atoms are arranged in an fcc sublattice, the oxygens 'atoms are in a bcc sublattice. One sublattice is shifted by a quarter of the body diagonal.

The crystal structure corresponds to the space group Pn3m, which incorporate a full octahedral symmetry. In the case of considering the oxygen atoms as the origin of the body centred cubic (bcc) primitive cell, the four copper atoms are located in the diagonals in the positions: (1/4,1/4,1/4), (3/4,3/4,1/4), (1/4,3/4,3/4), (3/4,1/4,3/4), as represented in the figure 1.2.

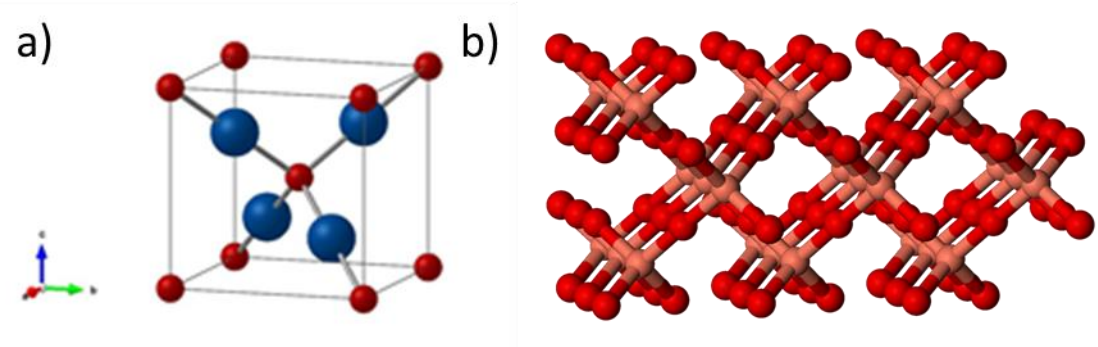

Figure 1.2 a) Cu_2O Crystallographic cell with oxygen atom as origin in the bbc cell. Oxygen are represented in red and copper in blue. (b) Cu_2O Crystallographic structure of 3x3x3 cells (In red copper atom and in pink the oxygen one)

As shown in figure 1.2a) the copper is directly coordinated with the oxygen atoms, while the oxygen is tetraedrically coordinated with the copper ones. The bonds' length between Cu-O neighbours is 1.85 Å, Cu-Cu bond is 3.02 Å long, while O-O has a length of 3.68 Å. This lattice produces an oxide with a density of 6.10 g/cm^3 and molar mass equal to 143.09 g/mol. The copper concentration is twice the oxygen one, 5.05×10^{22}cm^{-3} and 2.52×10^{22}cm^{-3} respectively. This values can be found in literature, such as Resende[1], Biccari[37],Sun[38] and Korzhavyi[34].

This material is been studied since the properties as p-type material, as described in the next paragraph, leading the possible creation of p-n junction[39] used in different devices as solar cell[40,41].

Moreover, it is already been studied by many authors and its deposition took place through the use of different techniques as electrochemical deposition[42 43], sputtering[44] and sol-gel spin coating[45,46].

1.3 Conduction in Cu_2O

This material has a direct bandgap equal to 2.096eV a room temperature. This energy gap would not let electron pass through so the copper oxide is an insulator in its stoichiometric composition.

The experimental values for the holes and electrons effective masses are 0.99m* and 0.58m* respectively, as reported by Korzhavyi[34].

P-type oxides are characterized by the fact that the valence band is mainly formed from the oxygen p asymmetric orbitals. The ionic aspect of the metal-oxygen bond leads the formation of a deep acceptor level, which limits the holes mobility. Among the different metallic oxides, Cu(I)-based oxides exhibit one of the lowest ionic character, therefore it is one of the most promising candidates as p-type transparent semiconductors. In figure 1.3a) it is possible to see the orbitals disposition and in 1.3b) there is the band diagram for this material.

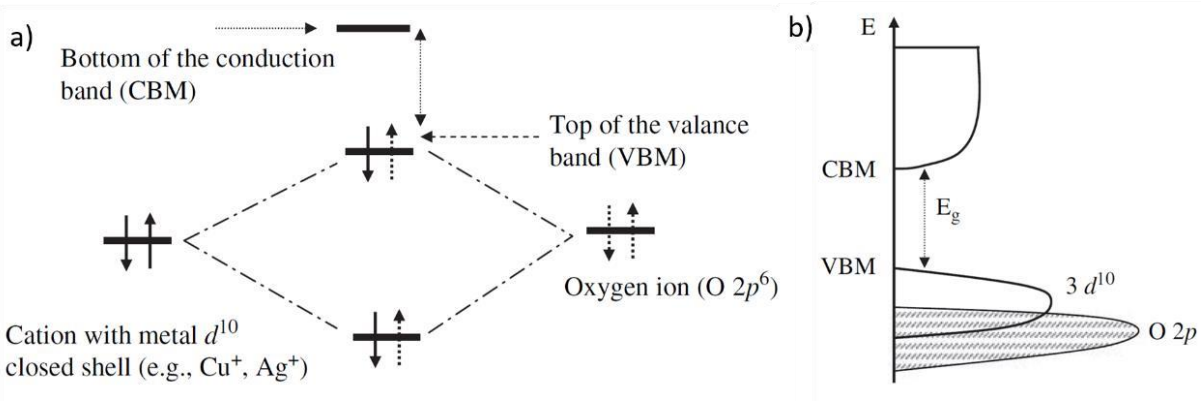

Figure .1.3 a) Orbitals disposition between an oxide ion and a cation with closed metal d shell for copper oxide b) Energy bands diagram for cuprous oxide. Obtained from H.Kawazoe[47]

This p-type conductivity arises from the intrinsic defects present in the crystal lattice, as explained next. Among all of them, copper vacancies are the ones able to generate holes, so responsible of the conduction. This because the removal of a copper cation will leave a negatively charged empty space, a vacancy, which will introduce a hole in the valence band creating a acceptor level above the top of the valence band.

In the copper oxide, these vacancies are of two different type. The so-called simple copper vacancies where one copper atom is missing leaving two oxygen atoms bond with three copper atoms, creating the vacancy. The other type, instead, are the split copper vacancies where a copper atom is removed and the absence of this leads a movement of the copper neighbour towards the vacancy. The moving copper atom will go into a tetrahedral site where will be bond with four neighbouring oxygen atoms. The two types of vacancies are shown in figure 1.4 on the left the simple vacancy, on the right the split copper vacancy.

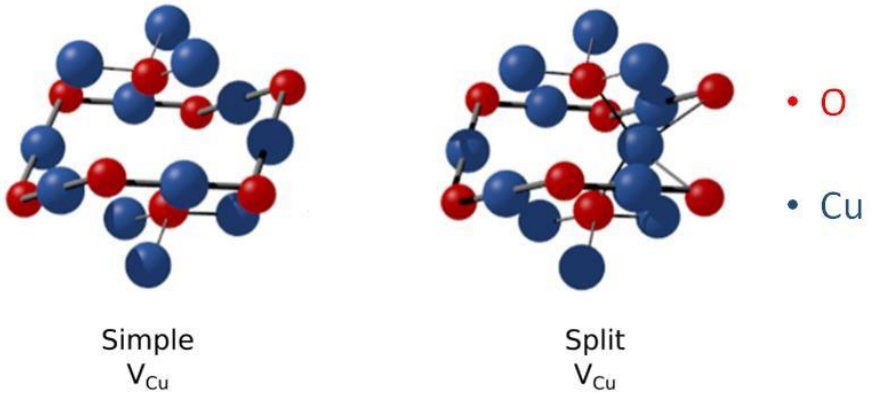

Figure 1.4 Two type of vacancies in copper oxide, on the left the simple copper vacancy and on the right the split copper vacancy. Adapted from Resende [1].

To better understand how conduction is influenced by this kind of defect, many authors performed DFT calculation on this system and as it arises from Isseroff[48], this is strictly related to how the hole localization changes based on the type of defect. Indeed, in the simple vacancies there is delocalization of the holes smeared through the Fermi level, while the split vacancies show a discrete trap level 0,57eV above the Fermi level. This fact, proved by Bader method in Isseroff[48], leads to the holes' localization on the Cu atom central to the defect in the case of split vacancy, whereas in the other case a negligible hole localization take place on the atoms surrounding the simple copper vacancy.

1.4 Copper oxide doping systems

Doping is the addition of a small percentage of foreign atoms in the lattice of the intrinsic material. The goal is to improve the material's properties modifying the structure of the intrinsic lattice and consequentially the bands diagram. This will lead to modification of the bands diagram with the possibility to arise new energetic levels able to participate to the conduction. The doping can be interstitial or substitutional, based on the size of the dopant atoms and theirs electronic valences.

Interstitial doping is done through the insertion of an atom with dimensions much smaller than the host atoms and so the introduced atom will occupy a position between two host atoms. Since theirs locations, they are electrically non-activated and theirs positions would lead to the generation of impurities levels which will behave as recombination centres, limiting the conduction.

The substitutional doping is performed when an inserted atom replaces the original host atom. In this case, the doping is done with atoms of a close size of the host one. Since they are incorporated inside the lattice, they act as electrically activated dopants atoms, so able to participate to the conduction as donors or acceptors, depending on which charge are they providing.

In this research framework the doping of cuprous oxide was done with larger cations than Cu^+ as demonstrated by ab initio calculation in Nolan[49]. These cations will deform the crystalline lattice, without loose the original cubic structure, increasing the band gap with a consequential improve in transparency, but as drawback there will be a reduction in the electrical conduction, i.e. more energy is required to let the electronic transition happen.

This improvement of the optical properties is dependent by the dopant, in fact as shown in Ye[50] , for the interstitial fluorine doping the energy gap is reduced while if fluorine is in a substitutional position this will make the Cu_2O metallic.

The doping effect on the cuprous oxide is been already demonstrated to be efficient with different type of elements, Mg[51], Sr[52], Co[53], Sn[9],N [8,18,54], Ag[55] and Bi[56]. The values reported in the table 1 are for different deposition techniques and conditions.

Many others authors has studied the possibility to doped cuprous oxide with different material as shown in Sieber[57].

Table 1 Reported dopant for cuprous oxide and relative values

Dopant	Amount of dopant (%)	Band-gap (eV)	Resistivity (Ω.cm)	Mobility ($cm^2.V^{-1}.s^{-1}$)
Pure copper oxide[25]	**0**	**2.09**	**100**	**6.8**
Magnesium[51]	**50**	**2.2**	**11**	**5**
Strontium[52]	**5**	**2.2**	**1.2**	**15**
Cobalt[18]	**5**		**512**	
Tin[9]	**9**	**2.2**		
Nitrogen[22]	**1.7**		**0.2**	
Silver[26]		**1.2**	**0.2**	**24**
Bismuth[24]	**7**	**2.17**	**1e6**	

As shown from these values, the effect of the dopant varies with the nature of the incorporated element, which will influence in different way the lattice structure, the crystal growth and consequentially the different properties of the material.

From these results, this experimental research is based on the study of the growth and characterization of mainly Tin doped Cuprous oxide(Sn/Sn+Cu) and as exploratory study of Lithium doped phase CuLiO, deposited both, as explained in the next chapter, by AA-MOCVD.

This technique consist in the deposition through chemical reaction of a vaporized solution, which is mainly composed by a solvent and chemical precursors. In these precursors, the element that will be deposited, is linked with other atoms through a different number of bonds according to its oxidation state. This parameter will influence the phase's growth of the deposited film and a possible change of the oxidation state can occur during the deposition.

The aim of this research is to study the influence of five different tin chemical precursors on the properties of the cuprous oxide phase and how the oxidation state of the tin is modified, knowing the initial one in the precursor, during the deposition.

Furthermore, the interest of the conducted investigations, is to understand the incorporation process for the different precursors and this is been done probing the amount of tin in the layer starting from a known one in the solution.

To verify an enhancement of the film's properties different test were performed, trying to understand how the tin doping can vary the morphology and the structure of the deposited layers and how these change with the different tin precursors.

The effect of different doping level of tin is also tested, checking how the different concentration of tin precursor in the solution modify the incorporation of this material in the film, modifying the structure and the morphology of the deposited film.

The main purpose of this part of the research is to find the optimized amount of tin, with an established precursor, the Dibutyltin Diacetate (DBTD), which can improve the properties of the film leading to an enhancement of these with respect to the intrinsic case.

Furthermore, as shown in chapter V, also the effect of the lithium as dopedit is been tested. In this context, fewer depositions took place and this study case is limited in terms of dopant concentration and only one lithium precursor was tested, the lithium (II) acetylacetonate.

The obtained samples were characterized with the same tools used in the tin doping case and the intrinsic one and the results are shown in the relative part of the chapter V.

2. Experimental Setup and Characterization Procedure

2.1 Aerosol-Assisted Metal Organic Chemical Vapour Deposition

At the Laboratoire des Matériaux et du Génie Physique (LMGP) in Grenoble, different types of chemical vapour deposition (CVD) processes has been studied and developed. The chemical vapour deposition is defined as a chemical reaction between reacting species, provided as vapour, in the neighbourhood of a heated rotating substrate, which results into the deposition of solid by-products on the surface. One of the main advantages of this process is the high reliability and the flexibility of this technique for the deposition. Moreover, it is able to deposit uniform and conformal film.

The Metal-organic chemical vapour deposition (MOCVD), a variant of this technique, is based on the deposition of materials starting from metal-organic precursors, which can be in solid or in liquid form. These precursors are organic molecules with metallic elements presenting metal-carbon, metal-oxygen-carbon bonds that are decomposed by a reactive gas in a thermally energetic environment, resulting in the formation of a solid material on the substrates.

In this study case, the copper precursor is the copper acetylacetonate, briefly called Cu (II) acac. This precursor is already been studied from many research groups as Chang[58], Resende[1] and Yuneng[59]. For what regards the doping with tin, many precursors have been studied to verify which one leads to the best performances in terms of electrical and optical properties. In the case of lithium as substituent, the used chemical precursor was lithium (II) acetylacetonate indicated with Li (II) acac.

The use of the MOCVD is motivated by the various advantages in materials processing, from the possibility to operate at ambient pressure obtaining a high uniformity up to the high quality of the layers. Moreover, there is the possibility to grow thin and conformal films composed by highly reactive sub-micron particles.

Furthermore, this technique is been studied because of the possibility to deposit at low temperature leading a reduction of the manufacturing cost and together with the use of low cost precursors and the big area deposition make this method industrially advantageous.

Another advantage of this technique is that it is able to deposit materials, at atmospheric pressure, which are difficult to transport via gases as shown in Tech[60]. Moreover, the possibility to prepare the mist from the mixture of different precursors as long the solubility and the chemical stability is granted, represents another advantage for this technique. This technique is already been studied for the deposition of oxide as shown in Fanciulli[61] and Moon[62].

The use of chemical solutions and the possible creation of volatile compounds represent one of the main disadvantages of this deposition method. Another drawback of this technique is the difficult stabilization of the aerosol flux during the transport of the vapour to the reaction chamber.

Among the different types of MOCVD techniques available, this research is based on Aerosol-Assisted Metal-organic Chemical Vapour Deposition (AA-MOCVD). This type of CVD process uses an aerosol medium to transport the vaporized solution into the deposition chamber. Furthermore this technique is already been used to grow oxide thin films as in Wrigth[63] and Song[64].

The complete scheme of the AA-MOCVD is shown in figure 2.1. In this figure the red arrows indicate where the gases enter. The partial pressure of Argon is four times the oxygen one, 6 l/min and 1.5l/min, respectively. An electronic controlled gas valve, as explained next, controls these fluxes.

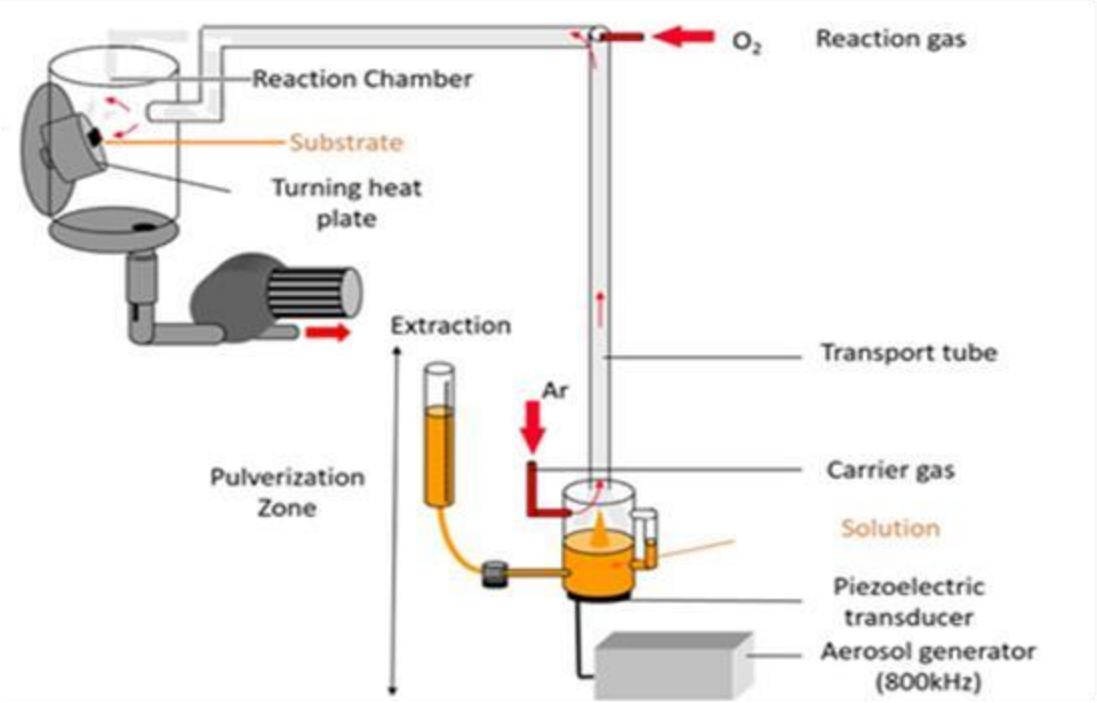

Figure 2.1 Aerosol-Assisted Metal-organic Chemical Vapour Deposition system. Obtained by Resende[1]

In this configuration if the flux is laminar, the flow arrives with a horizontal flux in the chamber leading a uniform distribution on the substrate. If it is turbulent, depending by many deposition parameters and by the geometry of the machine itself, the deposition can experience non-homogenous distribution on the substrate leading to a spatial thickness difference of the deposited films.

The horizontal flux is an optimization of this technique because, as demonstrated in the work of Resende[1], a vertical flow where the flux arrives from above the rotating heating plate, could lead the precipitation of macro drop of solvent or large undissolved precursor particles.

The next image, figure 2.2 shows a detail of the rotating heating plate where the holder is mounted and an IR picture token to analyse the heat distribution on the plate when the temperature was set to 350°C. The measurement through the IR camera was performed to verify the thermal homogeneity of the rotating plates such to guarantee the uniformity of the reaction when the vapour reacts with the substrates.

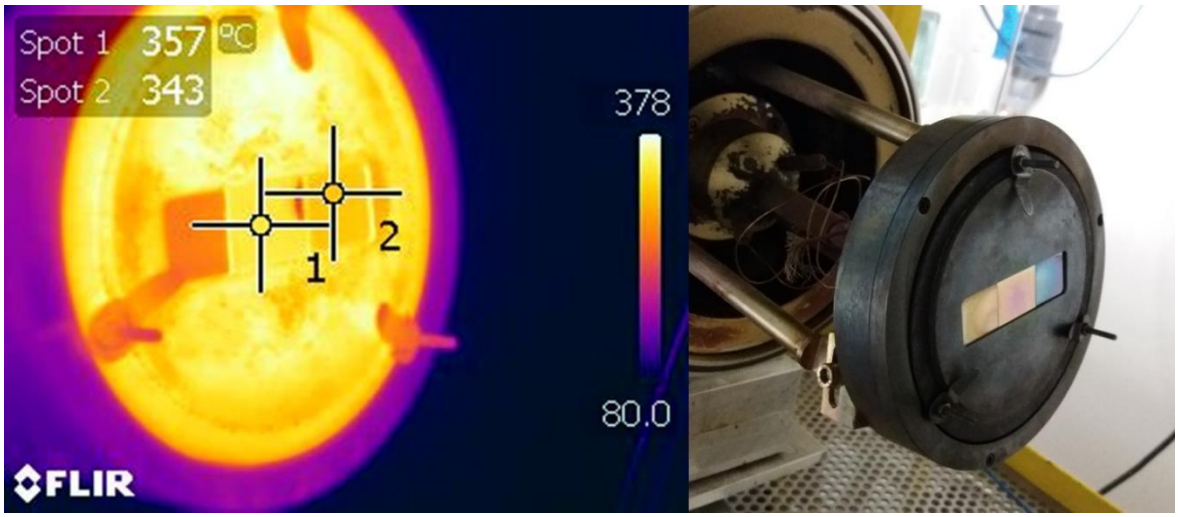

Figure 2.2 IR view of the rotating heating holder and its view at the end of the deposition.

2.2 Deposition experimental description

The first step of the deposition is the preparation of the chemical solution, that is produced by mixing the precursors and the solvent, ethanol. Ethylendiamine is added to increase the solubility, with a double concentration with respect to total molar solution concentration. Then the solution experiences a constant stirring a room temperature until a uniform mixture is obtained. In case of a doped material, the indicated percentage of precursor is always the fraction between the dopant molar concentration and the total molar concentration of all precursors in the solution, being presented as X%(Sn/Sn+Cu) as in the case of lithium X%(Li/Li+Cu). The mainly used precursors were in solid form and through the use of a balance and a simple chemical calculation, it was possible to determine the amount of dopant required to reach the wanted level of doping in the initial solution.

Furthermore, also the pH of the solution plays a fundamental role tuning the conductive properties of the cuprous oxide, establishing if it has a p-type behaviour or a n-type one as shown in Xiong[65], but in this research framework the effect of this parameter was not investigated

In the majority of the cases, alkaline earth boroaluminosilicate glass (Corning 1737), Microslide glass, and p-type silicon wafer were used as substrates. Generally, the Corning glass is situated in the middle while Silicon and micro-slides occupy the lateral positions of the holder as shown in the figure 2.3. The used glass substrate were bought in a rectangular of 1,5cm X 7,5cm so a cutting process was required to resize them. To perform this step the used tool was a diamond tip to incise the glass then with the use of pliers was possible to cut them in the wanted size.

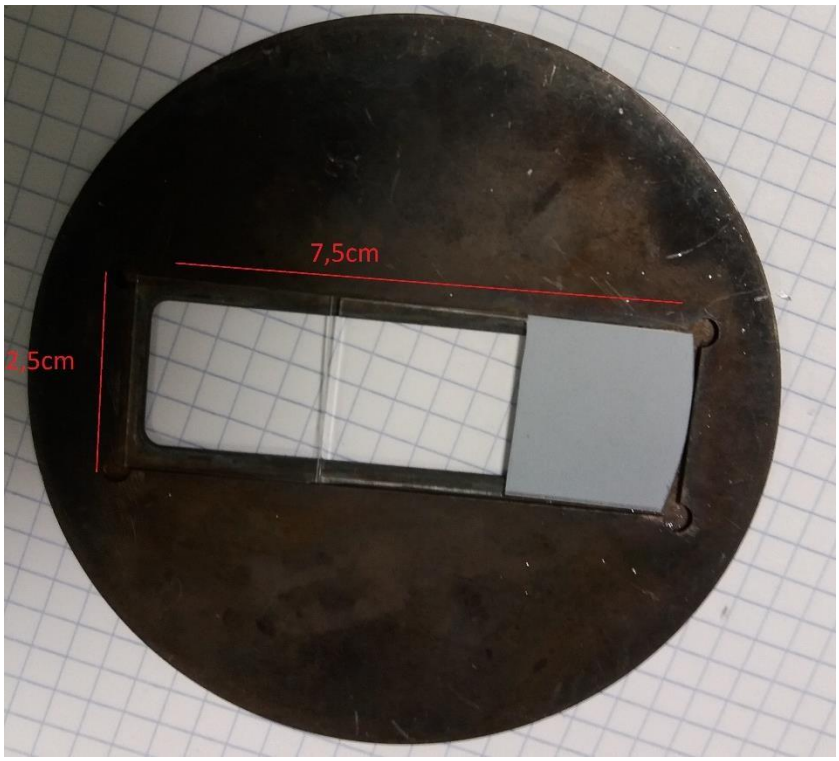

Figure 2.3 Disposition of the substrates on the holder next placed on the rotating heating plate from left to right: Microglass, Corning glass and Silicon.

The next step is the cleaning of the substrates to avoid all the possible contaminations reducing defects generating centre. This step is performed by a mechanical brushing using paper and a sequence of solvents with the following order: acetone, isopropanol and de-ionized water.

Finished the mechanical cleaning the substrates are subject to an ultrasonic bath in isopropanol for 15 minutes, then they are rinsed with de-ionized water and then dried using azote and placed in the holder as shown in figure 2.3. At this point, the holder is placed on the heating plate and the temperature starts to increase, controlled by the thermocouple and a thermos-coax.

The heating step lasts around 30 minutes. Before the deposition starts, the heating plate starts to rotate and the solution is spilled to a vessel connected to the piezoelectric transducer by a valve, as shown in the figure 2.4a). The height of the vessel allows the control of the solution quantity on top of the piezoelectric transducer.

The vibration of a piezoelectric transducer powered by a certain frequency, around 850 KHz, put the solution in resonance leading to the aerosol formation while a controllable power establish the desirable solution's consumption rate i.e. the volume of solution which is evaporated in a certain amount of time(ml/min). During this research framework, every deposition has a duration of 1 hour.

Once the mist is created, the aerosol is mixed with an inert carrier gas, argon, and with the oxidizing one, oxygen, and then the vapour is transported to the reaction chamber following the scheme of figure 2.1. When it arrives on the heated substrate, the thermal energy erases the bonds

between the metal and organic components, present in the precursors, leading to the subsequent interaction between the metal and the oxygen, then the deposition occurs.

The pressure inside the chamber is controlled by a barometer visible in the figure 2.4b) and the used pressure in the reactor was kept constant at 2.5mmH_2O during the presented depositions. The internal pressure of the chamber is controlled using a pump that is connected to a liquid nitrogen trap, used to collect the residual vapour reducing the organic contaminations in the film. The electronic gas valve shown in figure 2.4c) control the fluxes for the carrier and oxidizing gases.

The pressure, especially the oxygen partial pressure, has a strong influence on the crystal growth and it characterize which copper phase is going to form as explained in Tsur[53], Levitskii[66] and Nezar[67].

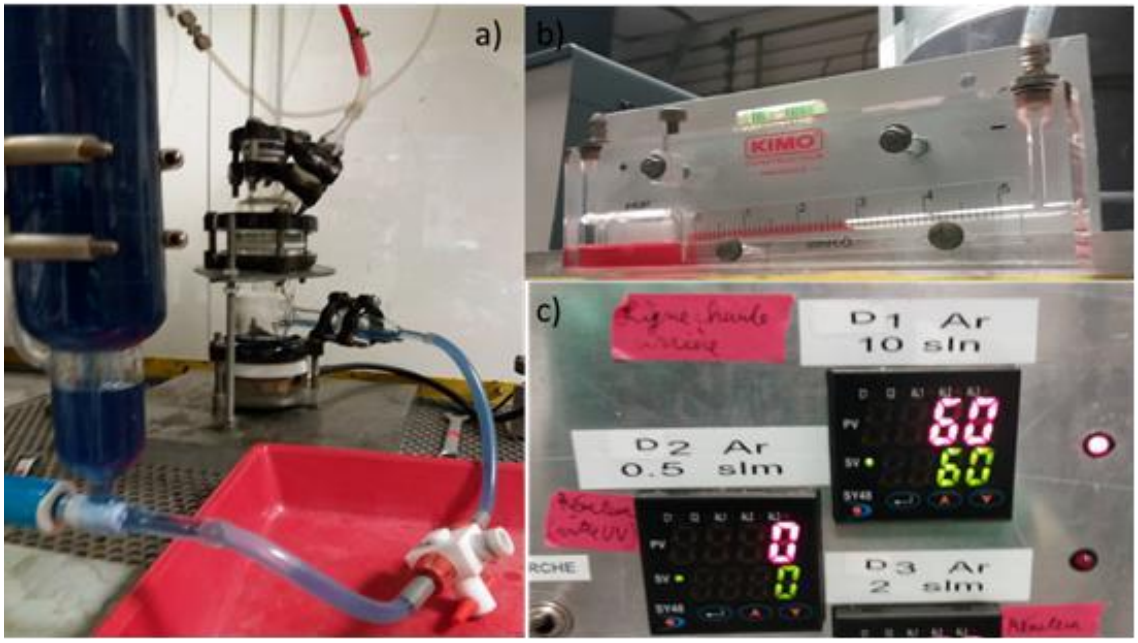

Figure 2.4 a) Vessel and piezo transducer connected through the valve. b) Barometer controlling the pressure inside the reaction chamber c) Gases valves controlling the flux of argon and oxygen

2.3 Characterization techniques

The main purpose of this Master thesis is to find a reproducible way to grow a layer of conducting and transparent material. Once the deposition took place, the analyses of the samples from the electrical, optical, compositional, structural and morphological point of view took place. To perform a complete characterization of the films different techniques were used, which will be describe in this chapter.

The presented results of this Master thesis are obtained through the use of these characterization tools.

2.4 4-probe measurement

Using this tool, the measurement of the sheet resistance took place and it is related to the resistivity ρ and to the sample's thickness, t, through the relationship:

$$R_S = \frac{\rho}{t}$$

This step was used to characterize the samples from the electrical point of view. The measurement was performed shifting the samples by probing these in five different points, the centre and the four corners. The values shown for the samples in this Master Thesis are the mathematical average of these values. The 4-probe system is shown in figure 2.5

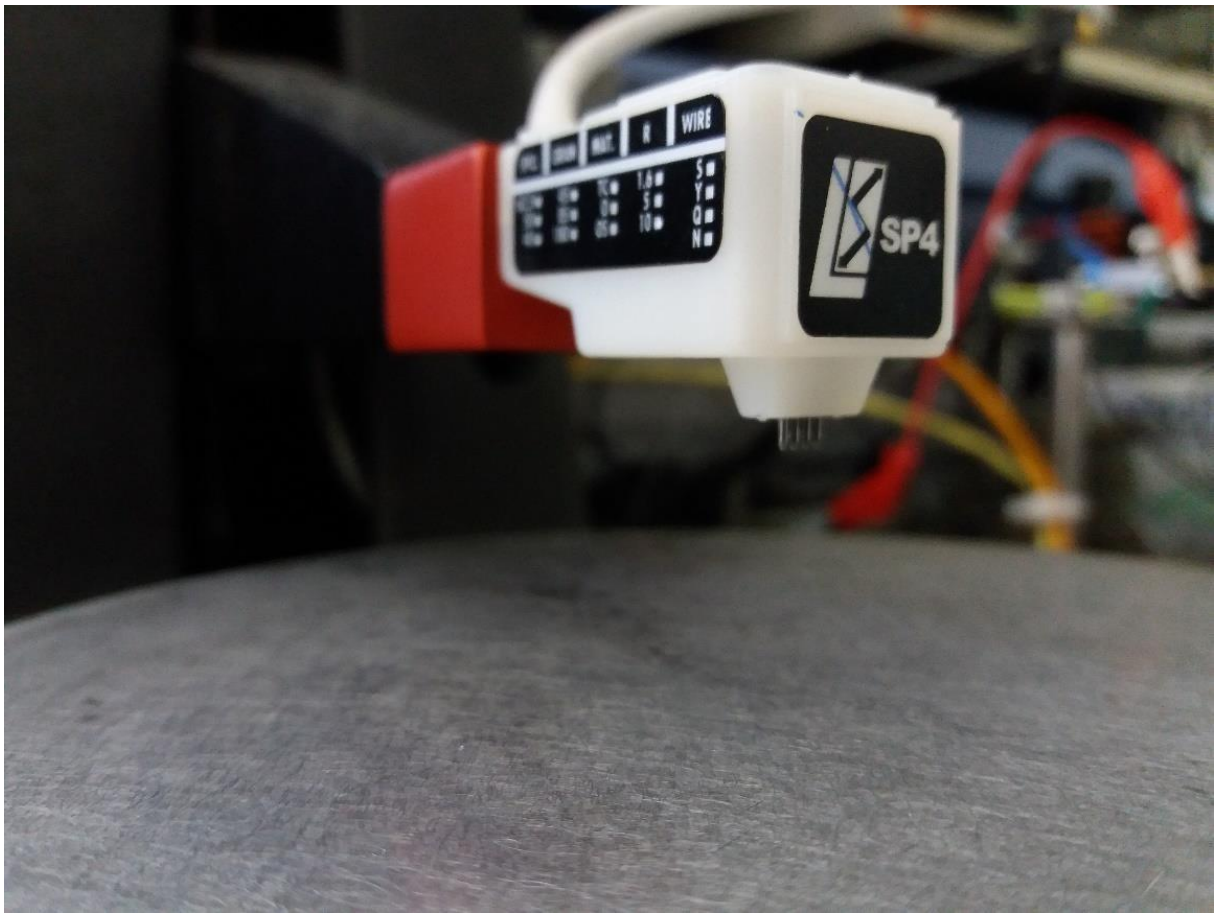

Figure 2.5 Four probe lever for the sheet resistance measurement, the samples is shifted to measure the electrical properties in five different points

2.5 Optical transmittance

The used measurement apparatus was a Lambda 950 spectrophotometer from Perkin Elmer. This system was used to probe the optical transmittance of the samples in the range between 250nm and 2500nm. The measurements were performed through an incident ray on the sample and the transmitted part of the light was collected in a detector, which compares the obtained intensity

with a previously measured baseline. In the range of the probed wavelength the system used different emitting sources and in some of the presented result can be noticed a peaks in the transmittance spectrum due to the switch of these lamps.

2.6 X-ray photoelectron spectroscopy (XPS)

This technique is able to probe the sample's surface and analyse the energy of the bonds between atoms. The surface atoms are ionized when an X-Ray impinges the sample. This will lead to the emission of an electron from the ionized atom and measuring its kinetic energy E_k, previously knowing the X-Ray energy $\hbar\nu$, it is possible to determine the binding energy E_b following the relation.

$$\mathbf{E_b = h\nu - E_k}$$

Each element of the sample, shows a characteristic binding energy corresponding to the atomic orbital from which is been emitted. Therefore, for each orbital there will be a peak in the XPS spectrum.

This information is used to verify the tin oxidation state, detecting which phase is formed during the depositions as shown in chapter IV for the tin doped copper oxide.

2.7 Scanning Electron Microscopy (SEM) & Energy Dispersive Spectroscopy (EDS)

This technique probes the sample with a beam of electrons created by an electron source by thermionic effect or by field effect emission. The most common SEM mode is detection of secondary electrons emitted by atoms in the layer excited by the electron beam. Collecting the secondary electrons using a special detector, an image displaying the topography of the surface is created.

Moreover, this technique can be also used to estimate roughly the samples' thicknesses through the use of the so-called SEM cross section observations, thus disposing vertically the samples and measuring the distance between the substrate and the edge of the film.

These measurements are not reported in this work because of the lack of consistency of obtained data.

This microscope was also able to perform EDS characterization, so roughly estimated the nature and the amount of elements composing the films. The SEM system is shown in 2.6 a) and the EDS probe is visible in 2.6 b).

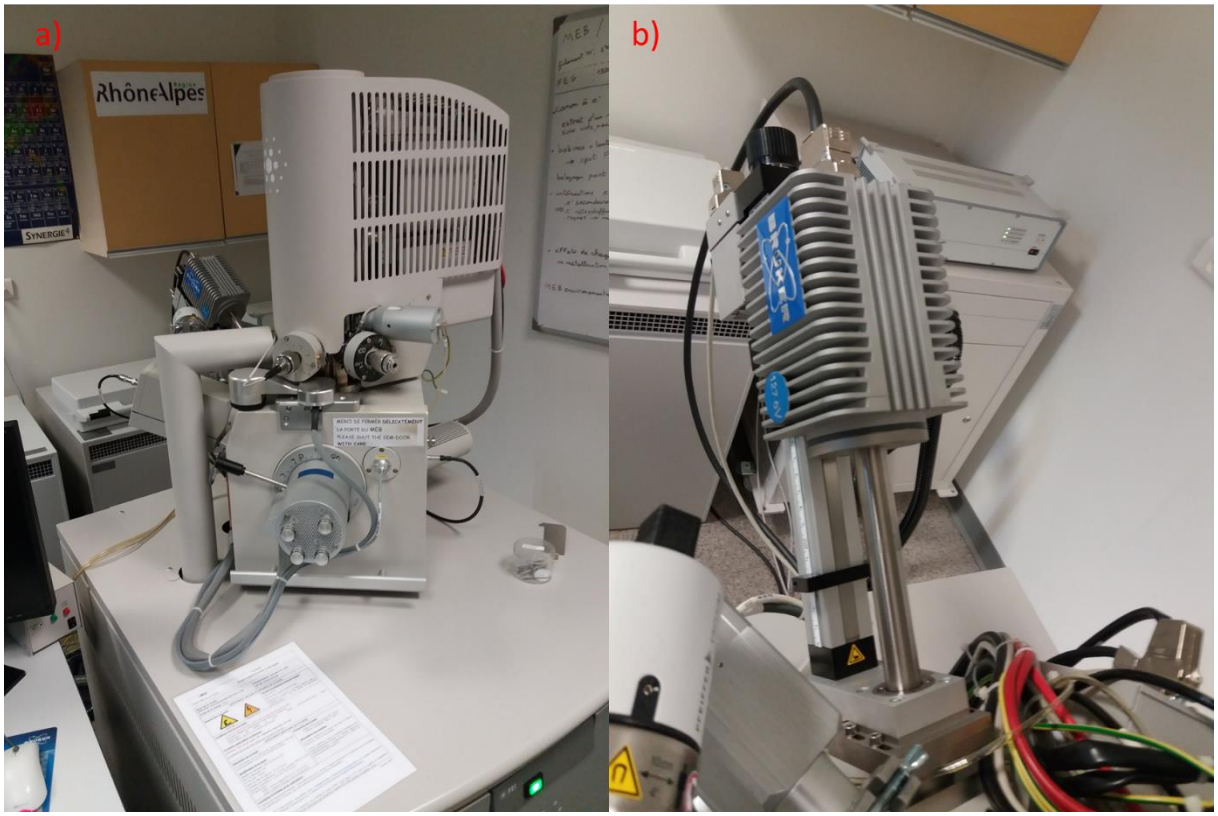

Figure 2.6: a) Scanning Electron Microscope tool b) Electron Dispersion Spectroscopy probe

As will be shown in the results part this technique is been used to evaluate the incorporation of tin as dopant in the film. Moreover, this kind of measurements are influenced by the atomic weight of the studied element. In the case of Lithium, due to the electronic configuration of this element, these measurements are not possible.

2.8 **Raman spectroscopy**

This technique is based on the Raman scattering, an inelastic scattering where an imping photon excites the molecules to higher energy. It is able to detect the different composition of the film through the energy difference obtained by the interaction of the photon and the studied material. Indeed, the decay of the excited electron belonging to the material will result in a shift in energy that will be detected by a sensor and measured. This energy difference is equal to the difference between the initial and the final vibrational state and generally if the final state is higher in energy than the initial state, the scattered photon will be shifted to a lower frequency (lower energy) so that the total energy of the system is conserved. This shift in frequency is called a Stokes shift. If the final state is lower in energy, the scattered photon will be shifted to a higher frequency, which is called an anti-Stokes shift. Both the phenomena can be detected by the measuring instrument.

These measurements are afflicted by many factor as the varied intensity of the light source and from the environment in which they are performed.

During this study case, the source was a monochromatic ray in the visible range, the analysis where performed through a blue laser (488 nm). The wavenumber of the diffused photons, were analysed from around 50 cm^{-1} up to 1850 cm^{-1}. The laser light interacts with the material and the shift in energy determines the nature of the bonds created in the film leading to the formation of the so-called Raman spectrum.

2.9 Thermal Annealing

After depositions took place, the study of the effect of a thermal treatment is been performed, looking for the generation or activation of more vacancies improving the conductivity as explained in the chapter I and as shown for the magnesium doped copper oxide case as in Resende[1]

To perform this kind of study the first step was the measurement of the sheet resistance of the as-deposited samples, then using the system visible in the figure 2.7, the sample experiences a programmable and controllable increment in temperature thank the use of a laptop. Then the sample was kept at constant temperature for a certain time, 1 hour, and the temperature was then decreased. During all this process the resistance was measured by a multimeter in real time. Once the thermal cycle ended, another measurement of the sheet resistance occurred to verify a possible enhancement of the sample's electrical properties.

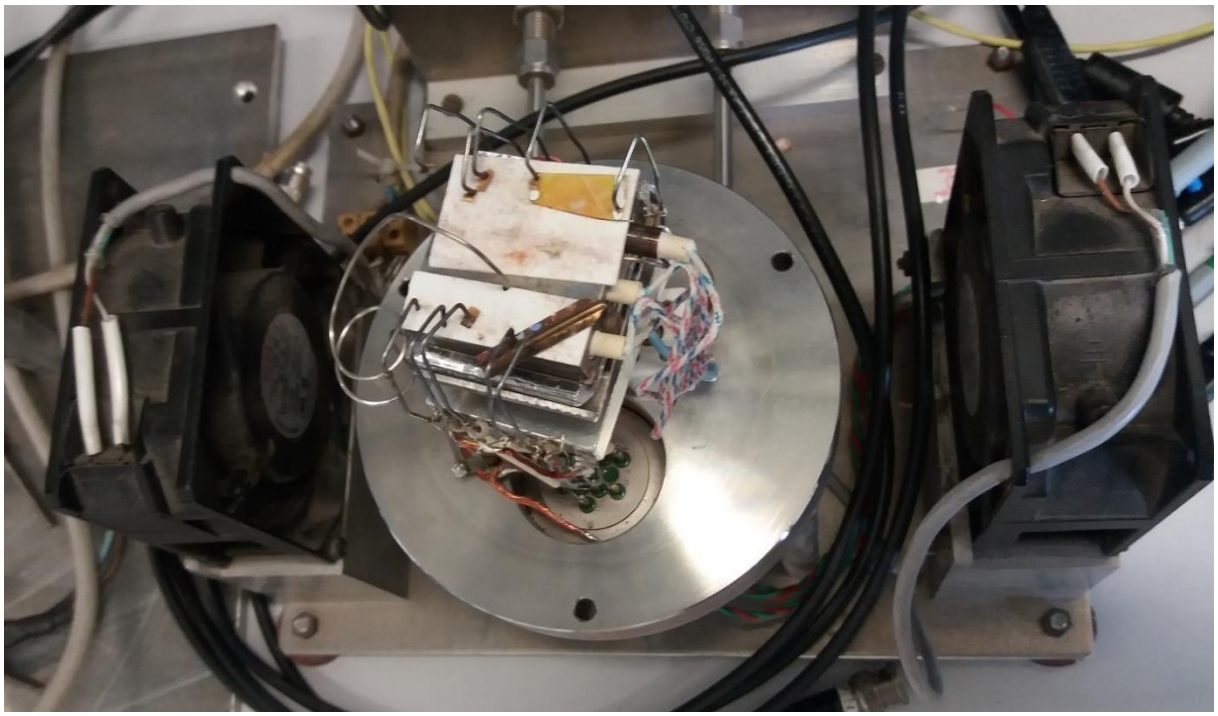

Figure 2.7: Thermal annealing plate, with sample connect to the 2 probe system

During all the cycles, the resistance is constantly measured thanks to a 2-probe measurement system, getting the possibility to track the behaviour of the resistance with the temperature and the time as shown in the relative result part.

3. Pure copper oxide deposition

In the framework of the study of the deposition of intrinsic copper oxide as p-type semiconductor through the AA-MOCVD method, the used copper precursor was Cu (II) acetylacetonate**,** which has a molar mass equal to 261,79 g/mol in solid form. In this compound, the oxidation state of the copper is +2. This precursor is already been studied and used to deposit copper compounds and their oxides as demonstrated in Nasibulin[68,69], Chang[59] and Kenvin[70].

Keeping in mind that the wanted copper oxide phase is the cuprous one i.e. Cu_2O, a change in the oxidation state from +2 to +1 should occur during the deposition.

At the beginning of this research, the main purpose was to improve the film's properties through the optimization of the deposition's conditions starting from the already obtained results in the LMGP laboratory. Many parameters has been modified to perform this optimization.

The first of the varied parameters was the solution consumption rate i.e. the amount of solution vaporized by the piezoelectric actuator in a certain amount of time. Then the effect of the total molar solution concentration was investigated.

This Master thesis is described in terms of the so-called precursor rate (mmol/min) i.e. the molar solution concentration (mol/l) times the solution consumption rate (ml/min). This parameter is been used to understand how much precursor is effectively injected in the deposition chamber and so to evaluate the real deposition rate linked with the original solution characteristic. The values assumed by the total molar solution concentration are 0,01mol/l and 0,02mol/l and the solution consumption rate is kept equal to 1,5ml/min or 2ml/min, calculated checking the solution volume in the vessel every certain amount of time, 5 minutes precisely. During the experiments, the deposition temperature was modified comparing the samples obtained at 350°C with respect to the ones deposited at 325°C, always with a deposition time of 1 hour. The argon volume was kept constant to 6l/min and the oxygen one to 1,5l/min. The pressure difference related to atmospheric pressure was kept constant to 2.5mmH_2O.

3.1 Structural properties

The structural properties of the deposited films for the different deposition conditions are been studied through the Raman spectroscopy technique. This characterization tool is already been used to study this compound as shown in Taylor[71] and Dawson[72]. As explained in Sander[73], the spectrum of Cu_2O is dominated by a high infrared activity as shown in the following measurements.

In figure 3.1, there is the comparison on how the deposition temperature and the precursor rate influence the structure of the deposited films and how these influence the Raman spectrums and the intensity of the peaks.

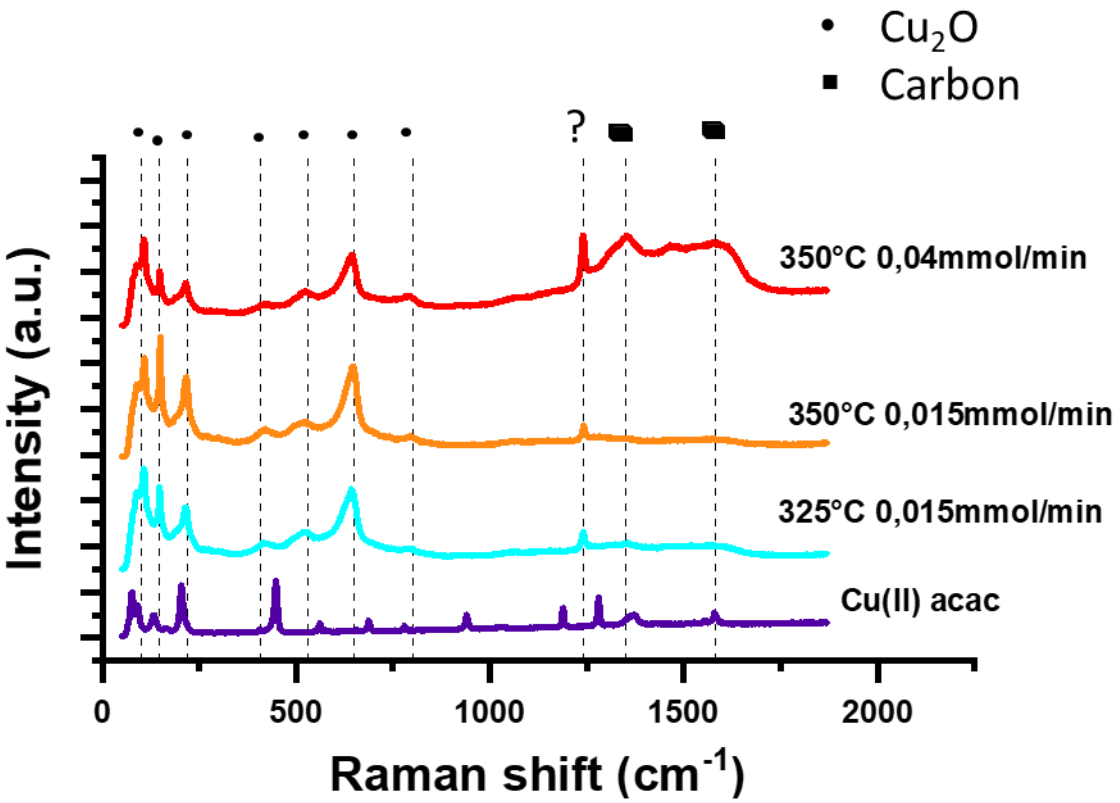

Figure 3.1 Raman quantification of pure Cu_2O thin films for the different deposition conditions

The deposited layers show quite similar spectrum in the low frequency range and these peaks are attributed to the Cu_2O phase. The differences in intensity can be related to the difference in thickness of the samples, which can influence the Raman spectrum. This parameter should be took in consideration during these measurement in fact the interaction volume of the laser beam can be higher than the sample thickness leading to the presence of peaks related to the substrate.

The highest organic contaminations are presents in the sample deposited at 350°C with a precursor rate of 0.04mmol/min, visible in the peaks at wavenumbers higher than 1250 cm^{-1}. The comparison between the cases deposited with a deposition temperature of 350°C reveals increased organic contaminations when a higher precursor rate is used. This could be a proof of the fact that a higher precursor rate leads a higher content of organic compounds present during the depositions. This could be related to the fact that more material reaches the substrate for the same unit of time leading to greater difficulties to erase the organic contaminations. The comparison of the temperature effect is possible in the case of precursor rate equal to 0,015mmol/l and in this case the Raman spectrum is similar in the samples.

Moreover, no significant Raman shift is present and, being this parameter related to the amount of stress in the film, it is possible to evidence that the different deposition conditions lead to the same amount of stress in the layer.

Another relevant element from the Raman spectrums is the presence of an unknown peak, at around 1250cm^{-1}, which is not reported in literature. This unknown peak will be present also in

the tin doped case and in the lithium one as illustrated in the next chapters. As reference, we put the Raman spectrum of the copper precursor, which present a higher number of peaks with respect to the films and as it is possible to notice the unknown peak is not present in this compound. For this reason, this peak could be attributed to the deposition.

3.2 Morphological characteristics

In this section, the surface of the samples is analysed, described in terms of the precursor rate (mmol/min). The study was performed analysing the effect of the different deposition conditions with a deposition time equal to 1 hour and a pressure of 2,5mmH_2O with the partial pressure of 6l/min and 1,5l/min, for argon and oxygen respectively.

To study the morphology of the samples, first information were obtained from the colour of the samples and from their macroscopic aspect. This parameter was evaluate by the samples' surfaces deposited on Corning glass. Through the use of the table in Bruhat[74],the colour of the samples was connected to the optical path and dividing it for twice the refractive index of the cuprous oxide, n=2.5, in the middle of the visible range (600nm), an estimation of the thickness is obtained.

These roughly estimated values are reported in figure 3.2 with the relative samples' surface. As trend, the thickness is reduced for the lowest temperature with respect to the case where deposition occurs at 350°C and clearly a lower precursor rate leads to thinner films. It is important to keep in mind that these values are roughly estimated and further characterization are necessaries, as ellipsometry, profilometry of the surface, Atomic Force Microscopy or SEM imaging of the cross-section. With this last technique, the group started some characterization of the films' thicknesses but they are not reported here because of the lack of consistent number of conducted tests.

The samples' thickness was also qualitatively probed through the transmittance tests and the refraction phenomena, which can provide an idea of this parameter, as it is possible see in the paragraph 3.4 of this chapter.

With these information, the study of the surface was performed, keeping in mind how the thickness of the sample can influence the growth of the grains and their size and how the growth varies depending by many others factor as deposition conditions and by the material itself.

Investigating the morphology of the sample through figure 3.2, is possible to notice that, comparing the case of the lowest precursor rate, the higher temperature leads to a higher thickness with significant variation in the grain size.

The used magnification is 50000X while these tests are been conducted.

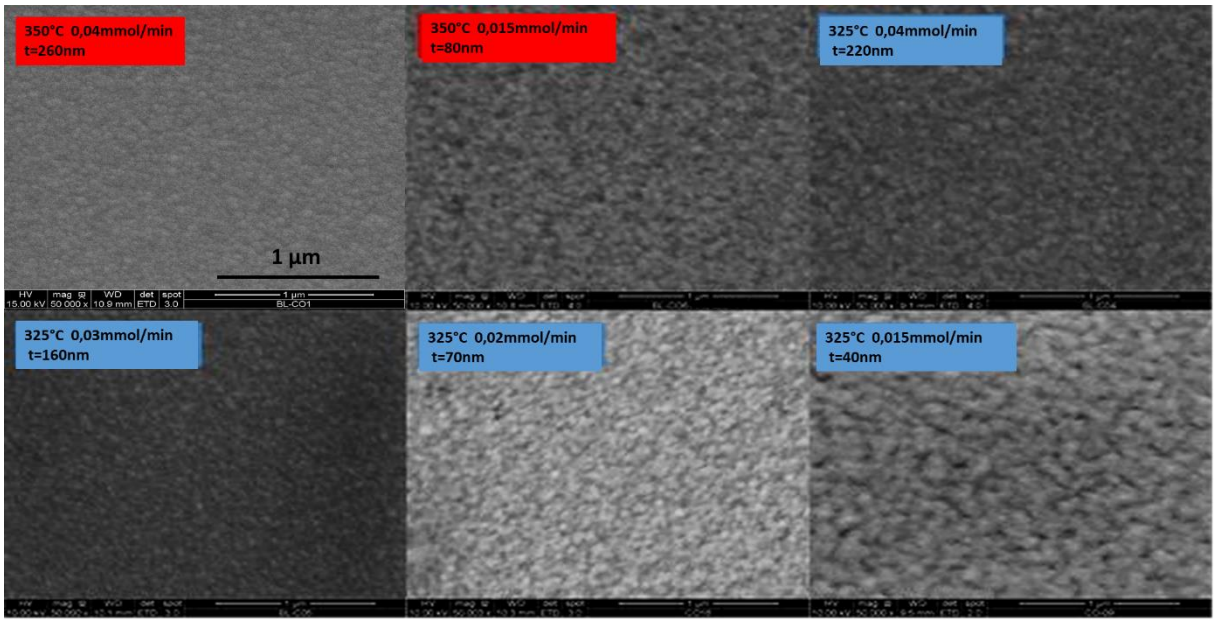

Figure 3.2 Surface of pure copper oxide in the different deposition conditions and relative observed thickness values observed with a magnification of 50000X

From figure 3.2, it is clear how the use of a lower precursor rate is linked with a reduced thickness. This is mainly due to the fact that, since the deposition time is always set to 1 hour in all these cases, the use of a lower precursor rate leads to a decreased amount of material reaching the substrate for unit of time. This has a clear effect on the thickness of the samples, indeed reducing the precursor rate there is a reduction of the thickness.

A reduced precursor rate, linked with a lower amount of material reaching the substrate will lead to a more effective elimination of the organic species, as proved by the Raman spectroscopy. The reduced quantity of material arriving the substrate per unit of time will lead the coalescence of smaller grains, increasing the grains size. Therefore, this will lead to thinner film with bigger grains size and lower organic contaminations, as proved by the above images.

When a higher precursor rate is used, an increased amount of material is able to reach the substrate and the organic species' rejection is more difficult. This will allow the growth of small grains not able to coalescence and thus it is not possible to increase the grains' size. Therefore, this will lead to a thicker film, more organic residues and, generally, a smaller grain size.

3.3 Electrical properties

In this section, the electrical properties of the as deposited films are investigated. As already explained in the chapter II, these values are the averages of the measurement performed through the 4-probe method measured at the centre and the four corners of the sample. These values were obtained fixing the thickness of the samples equal to 100nm during the 4-probe measurement. More accurate measurements of the thicknesses are mandatory to link these values with the resistivity of the films.

As shown in figure 3.3, the best values in terms of sheet resistance are obtained for the lowest temperature and lowest precursor rate of 0,015mmol/min i.e. when the solution concentration was equal to 0,01mol/l and the consumption rate is equal to 1,5ml/min with values close to 20MΩ/sq.

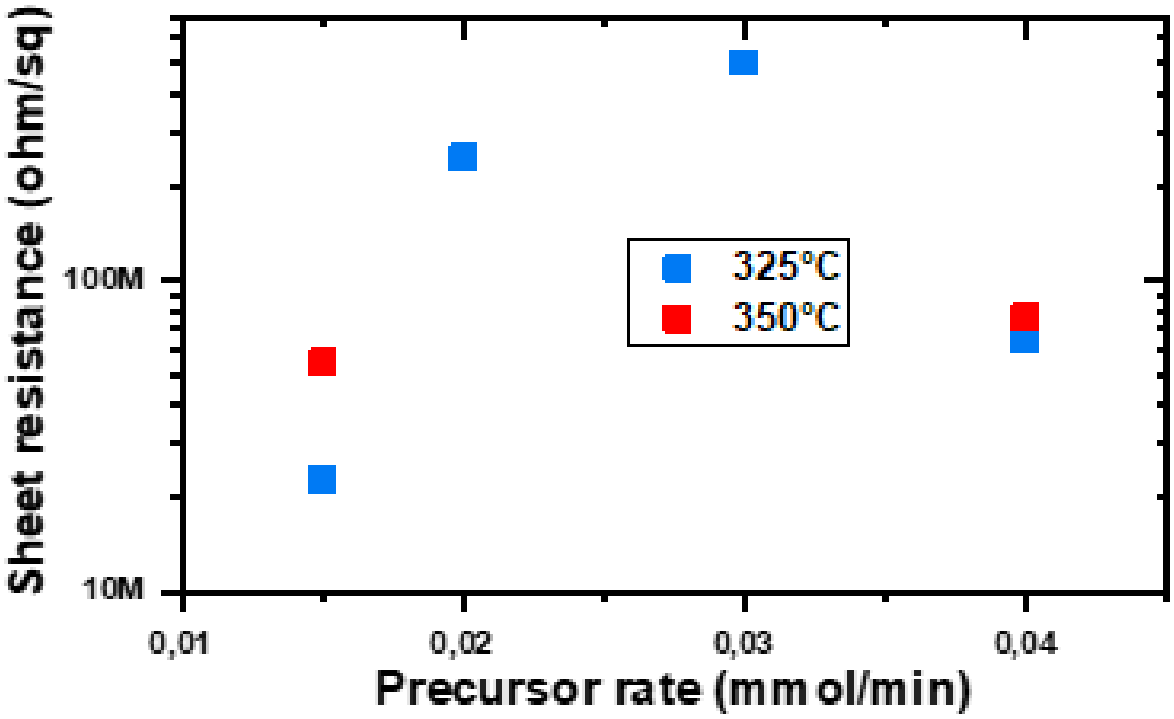

Figure 3.3 Sheet resistance for the different deposition conditions.

Furthermore, the use of a higher temperature leads to higher values of the sheet resistance and this difference is bigger as the precursor's rate is lower, maybe due to the different grains size as proved in figure 3.2 and the different amount of organic contaminations as proved by Raman. Since during these measurements, the films' thickness was not the same, these values could give an idea of how the deposition conditions can influence the resistivity of the films, recalling the relation between sheet resistance and thickness as explained in the section 2.4. In fact, for a stable quality of the film when the thickness decreases the sheet resistance increases. But in the deposited samples at 325°C by decreasing the thickness according to the precursor rate, first it is possible to observe an increase of sheet resistance and then a sharp decrease corresponding to an increase in the quality of the film so in the conductivity. This improvement is in good agreement with the reduction of organic contaminations analysed by Raman and also with the increase of grain size observed previously by SEM.

The increased values of sheet resistance shown by the samples deposited at 350°C it is also due to the higher presence of organic species, as proved by the Raman spectroscopy, which limit the electrical conduction.

The reduced value of sheet resistance can also be due to the different number and thickness of the grains boundaries. These can be seen as defects that limit the electrical conduction. Thus, bigger

grains, leading to a reduced number of grains boundaries, will improve the electrical performances of the films, as shown from the SEM image in figure 3.2 and proved by the sheet resistance values in figure 3.3. This point is still a controversial point in the oxides conduction theory as explained in Deuermeier[75], where there are highly conductive grains boundaries, surely the less organic contaminations are present, the more conductive the material will be.

From these results the optimized deposition conditions were found, which will be used as starting point for the deposition of tin doped copper oxide and the lithium one.

3.4 Optical properties

From the optical point of view, the next graph, figure 3.4, shows the comparison in transmittance for the different deposition conditions for the pure cuprous oxide.

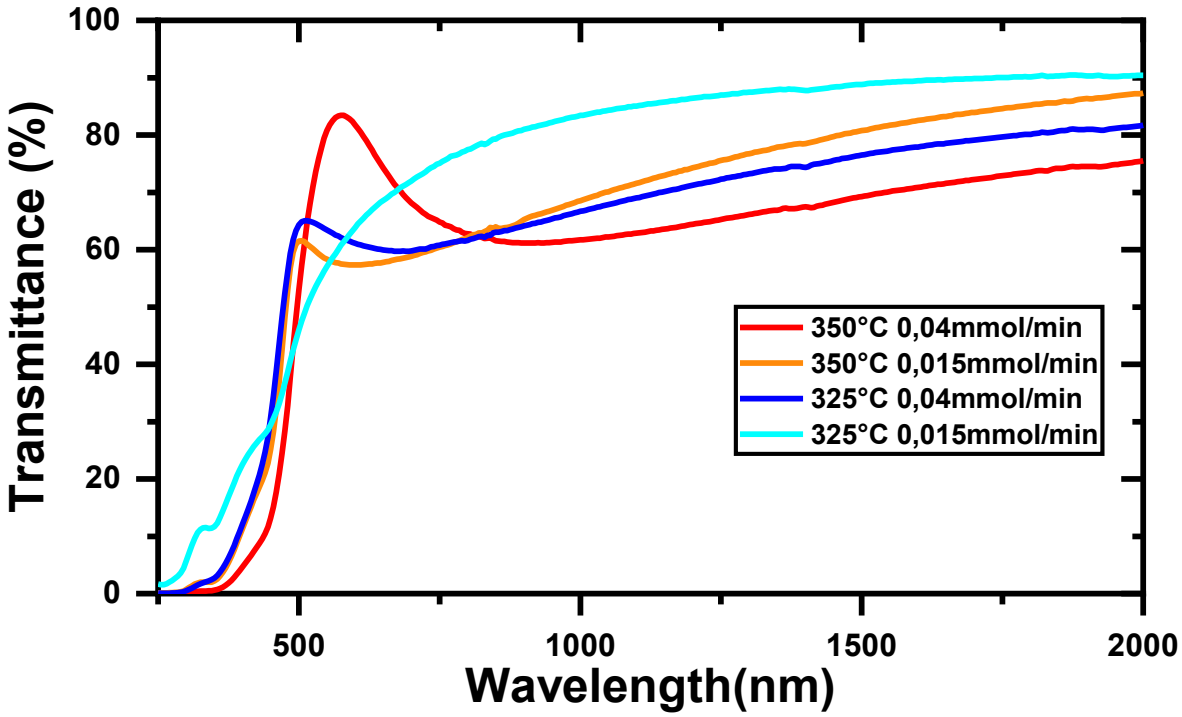

Figure 3.4 Transmittance spectrum in copper oxide for different deposition conditions

In this graph is evident that the spectrum is similar for the depositions with 0,04mmol/min as precursor rate and the difference in transmittance can be attributed to a difference in terms of thickness. The peaks of the spectrum in the visible range are due to refraction phenomena related to the samples' thickness. The sample deposited at lowest deposition temperature and lowest precursor rate present the lowest thickness, further confirmed by the fact that refraction phenomena does not occurs. The shift of the peaks with respect to the highest precursor rate and higher temperature may be due to the environmental sensitivity of the characterization tool.

As evidenced by these spectrums, the estimated values of the thickness are coherent with the transmittance values assumed in the IR. Thicker film will present a reduced transmittance and this is visible in figure 3.4 for all the studied samples. Indeed, the thinnest sample is the one that shows the highest transmittance in the IR field.

Others studies to better connect the transmittance spectrum with the thicknesses are required and other optical characterization such as absorbance test are necessary.

To better connect the optical and electrical properties, figure 3.5 shows the average optical transmittance in the visible range (390nm-700nm) with respect to the sheet resistance values, found with the 4-probe method.

As shown in figure 3.5 a lower deposition temperature leads a lower sheet resistance but this slightly influence the average transmittance reducing it. From this plot, the most interesting sample for this research is achieved from the samples deposited at lower temperature and the lowest precursor rate reaching values around 20MΩ/sq and an average transmittance in the visible range equal to 51%.

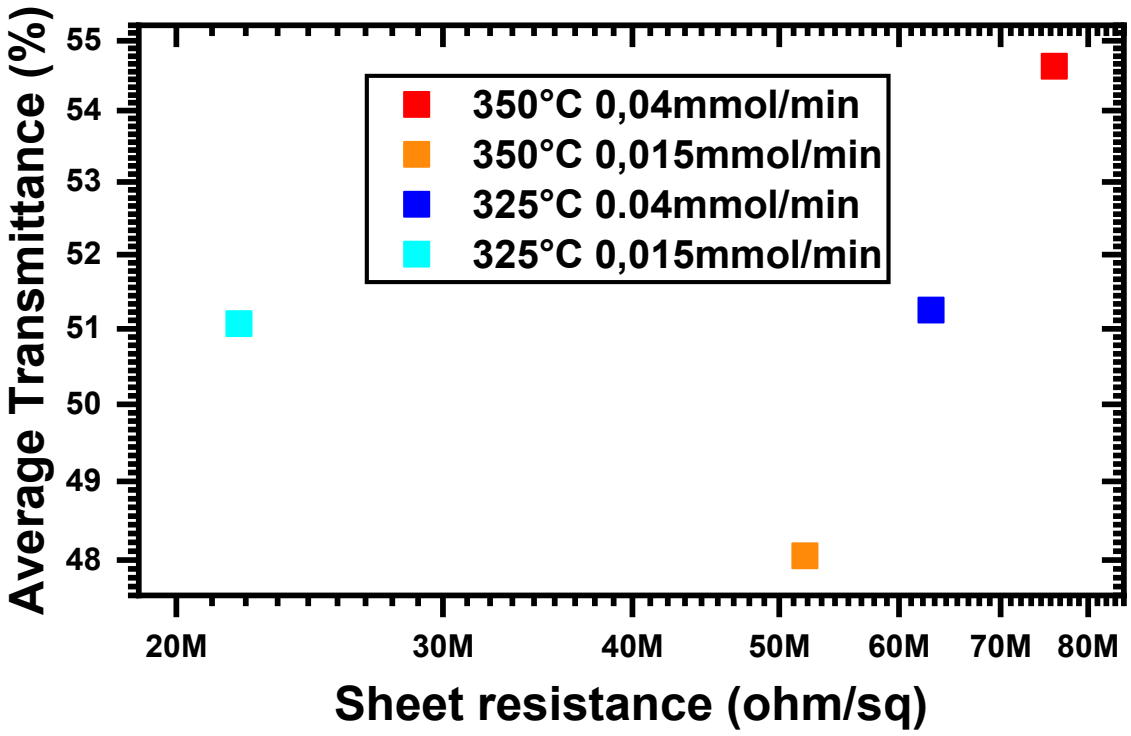

Figure 3.5 Average Transmittance versus the sheet resistance values for pure copper oxide samples deposited in different deposition conditions

As shown in the previous figure, the less conductive sample, around 80MΩ/sq, presents the best properties in terms of average transmittance with a value close to 55%, but this should be related to the samples' thickness.

Moreover, the graph shows a reduction of both the average transmittance and sheet resistance for a diminished deposition temperature when the precursor rate is 0,04mmol/min but this can be in relation with the different thicknesses shown. This kind of graph will be used to represent together both the electrical and optical properties for the others studied materials.

3.5 Thermal treatment

The research about the thermal treatment was done to investigate an eventual activation of the vacancies improving the conductivity of the film, as explained in the chapter II. Moreover, a thermal treatment could lead to a change in phase modifying the oxidation state of the element and this is generally related to a change in colour from the macroscopically point of view. Others modifications occur as change in the morphological, electrical, optical and compositional properties of the films as demonstrate in Berthomieu[76] and Siripala[77].

Furthermore, as explained in Akgul[78], the as deposited samples can be composed by a mixture of different copper compounds ,as cupric and cuprous oxide.

The effect of the thermal annealing is to change the relative concentrations of these phases that were found to be dependent on the annealing temperature

The annealing is also performed to study the thermal stability of the phase, so to verify how much the material is stable with the change in temperature, noticing if a phase change occurs, characterized by a modification in the macroscopic colour.

To explain better how an annealing experiment works in figure 3.6a) is shown the graph of the temperature variation with respect to the time experienced by the sample. In this study case, the annealing temperature was kept fixed to 250°C and the thermal treatment was 1 hour long in environmental atmosphere. This temperature was chosen to study the stability of this oxide trying to avoid cupric oxide formation.

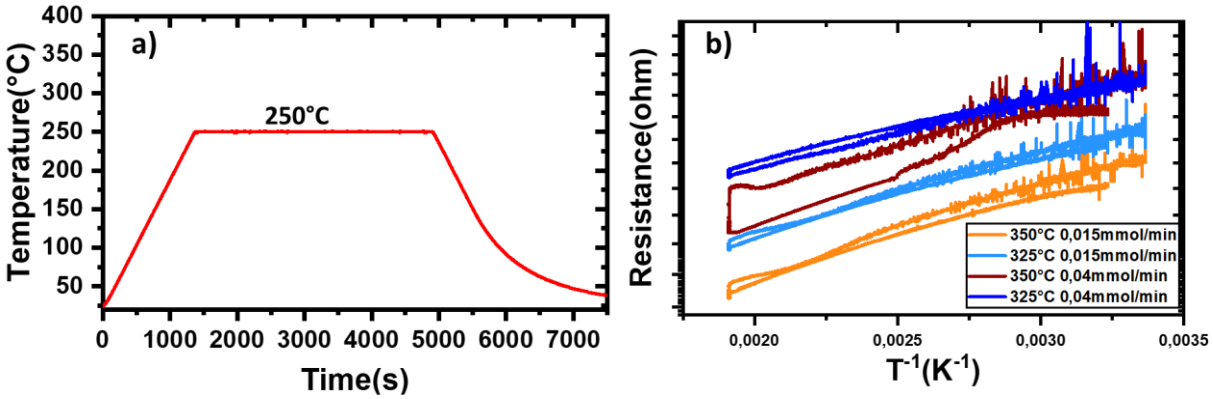

Figure 3.6 a) Temperature variation with time b) Resistance variation during the thermal annealing for pure copper oxide deposited in the listed different deposition conditions.

In figure 3.6b) there is the plot of the resistances' variation, plotted in natural logarithmic scale on the y-axis, with respect to the inverse of the temperature. These graphs are useful because clearly demonstrate a decrease of resistivity of the samples during the thermal cycle but they are used

mainly to calculated the activation energy, through the Arrhenius equation, from the slope of these curves. Linearizing around a certain value of 1/T, generally during the cooling down, it is possible to obtain an energy value that is related to the energy difference between the acceptor level and the top of the valence band. These values will be compared with the ones found with the ab initio calculation in Nolan[49] around 400meV for the vacancies activation. As possible to evidence in this graph, the resistance variation is higher when deposition occurs with a temperature of 350°C with a precursor rate of 0,04mmol/min, characterized by the increased vertical shift in the curve during the temperature plateau.

From these slopes, the activation energy was calculated during the cooling down and the values are reported in the table 2.

Table 2 Initial and final sheet resistance and respective activation energies for the different deposition conditions

Sample		Initial Sheet resistance (Mohm/sq)	Final Sheet resistance (Mohm/sq)	Activation energy (meV)
Deposition Temperature (°C)	Precursor rate (mmol/min)			
350	0.04	85	50	308.81
	0.015	47	31	275.72
325	0.04	87	78	253.66
	0.015	34	35	275.72

It is possible notice that the samples deposited with a higher temperature have values of activation energy that are generally higher and the reduction of the sheet resistance is higher for the case at 350°C, especially when the highest precursor rate is used. It is interesting to observe how the smallest precursor rate leads the same value of the activation energy for different deposition temperatures.

For the position of these acceptors levels with respect to the valence band i.e. the activation energies for these kind of defects, Nolan[49] reported 0.47 eV for V_{Cu}^{Split} and 0.23eV for V_{Cu}^{Simple} vacancies.

From the activation energies values in the table, it is noticeable that they are close to the reported ones for the activation of vacancies in copper oxide. As it is possible to see from this table there is a reduction in sheet resistance but the decrease is limited especially when a lower deposition temperature is used, as evidence by the practically constant value of the sample deposited at 325°C with a precursor rate of 0,015mmol/min. As conclusion, it is possible to notice that these values are in agreement with the already presented ones in literature as in Resende[1].

From these calculations, it is noticeable that the obtained values are slightly lower with respect to the one found in Nolan[49] for the split vacancies and this can also be related to the different used deposition conditions and moreover others investigation are mandatory to better understand how this parameter changes with the different deposition parameters. Another parameter that strongly influence the thermal treatment is the used annealing temperature and generally, as proved by this study and by Nerle[79], an higher annealing temperature leads to an higher activation energy but this is also connected with the formation of cupric oxide phase.

4. Tin doped cuprous oxide (Sn/Sn+Cu)

Tin doped cuprous oxide and effect of the different precursors

The interest in this research is based on the improvement of the films' electrical and optical properties through the tin doping. This study case has as purpose the analysis of the properties obtained thanks to the doping and the quantification of the amount of dopant in the layers, starting from the known one in the solution.

The oxidation state of the element influences the formation of the different compound during the chemical reactions. In the tin case when the valence is +2 stannous oxide is formed, while for oxidation state equal to +4 there is the formation of stannic oxide. In this study case, the starting oxidation state of the tin was known from the used chemical precursor and further investigations trough XPS would be necessaries to understand the oxidation state of the dopant in the compound.

As testify in Suh[80], the tin oxidation state in the used chemical precursor has an influence on the formation and growth of different compounds.

Many characterizations were performed to understand better the role of the tin as dopant and its impact on the different properties of the film.

Related to the effect of tin on cuprous oxide many research groups tested tin doped copper oxide as shows in the papers Kavitha[81] and Stengl[82]. Other studies demonstrate that the copper can be used as dopant for the tin oxide as in Tripathy[83] , Sakthiraj[84] and Roy[85]. This latter case bring to the formation of a n-type transparent conductive oxide as reported in Das[3] and Roy[85].

In this research framework, the main purpose is to evaluate and to understand the effect of the tin doping in the cuprous oxide deposition. After the deposition conditions 'optimization for the intrinsic copper oxide, different experiments were conducted to evaluate the impact of different tin precursors. In this study case Dibutyltin Diacetate (DBTD), tin(II) Acetylacetonate (solid), called tin(II) acac (solid), tin(II) Acetate, tin(II) Acetylacetonate (liquid), called tin(II) acac (liquid) and tin(II) 2-ethylhexanoate were tested. These experiments were performed with the same amount of tin in the initial solution, equal to 10% (Sn/Sn+Cu). During this work the precursor rate was kept fixed at 0,015mmol/min and the duration of every deposition was 1 hour with an exhaust differential pressure of 2,5mmH_2O, moreover the effect of two different deposition temperatures, 325°C and 350°C, is tested.

The results part is been split in two, the first one focused on the effect of the different precursors and the analysis of the obtained samples, followed by the second one where there is the presentation of the results obtained for the different amount of DBTD. To verify the effect of the concentration of the tin precursor, Dibutyltin Diacetate (DBTD) concentration in the solution was

varied, from 2.5% up to 70%, and a complete characterization of the samples occurred, as shown in the part 4.2 of this chapter.

In the latter not all the characterizations performed on the deposited samples will be presented for greater clarity.

4.1 Effect on the different tin precursors

The test on different chemical tin precursors is performed starting from the results obtained from the doping with DBDT. The amount of dopant is fixed at 10% of the total molar solution concentration. The presented results are for samples that have been deposited with a deposition temperature of 325°C, the used precursor rate is kept, equal to 0,015mmol/min, as in the optimized pure copper oxide deposition. In the electrical properties section, the effect of the different deposition temperatures is been studied, comparing the values of sheet resistances obtained for 325°C and 350°C.

4.1.1 Structural properties

From the figure 4.1, the Raman spectrum is presented for the samples where different tin precursors were tested.

The Raman spectroscopy shows that the cuprous oxide related peaks, the ones at low frequency, vary in intensity with the different tin precursors. The unknown peak is strongly reduced in the case of tin (II) acac (solid) while in the others cases is still present with different intensities.

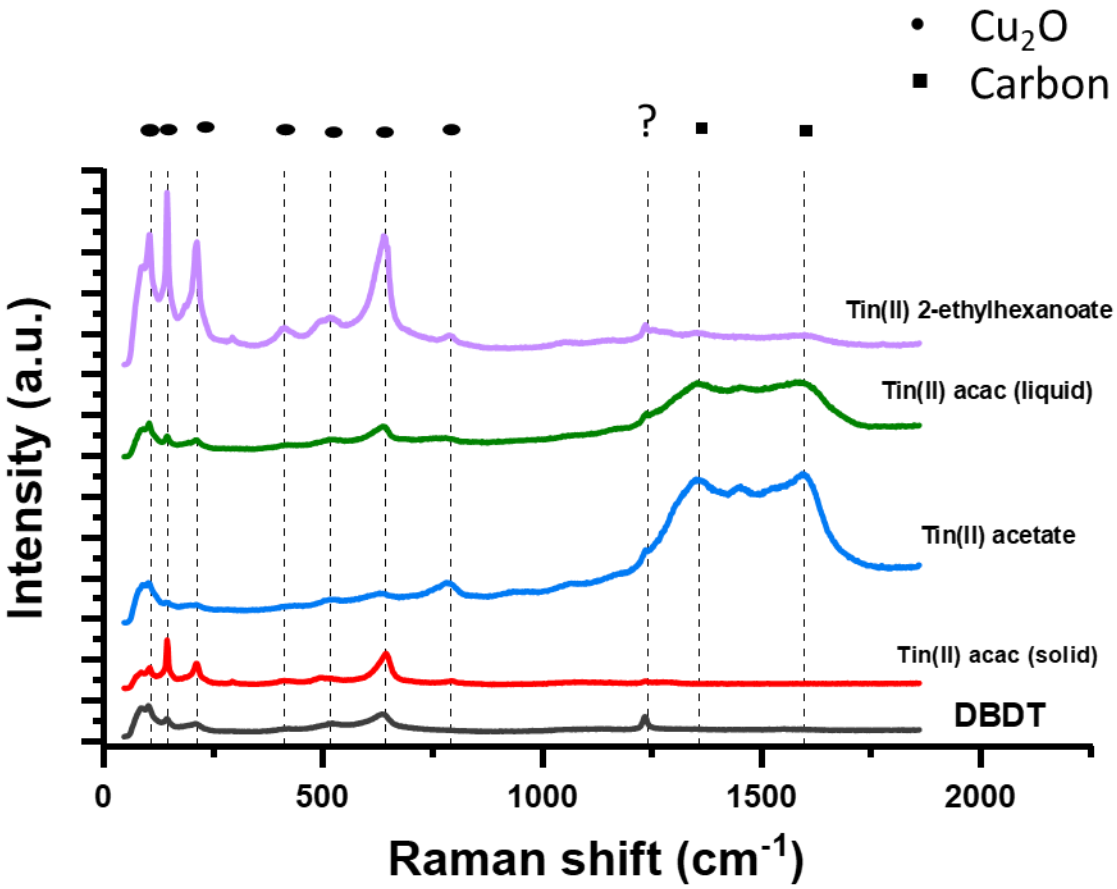

Figure 4.1 Raman spectroscopy for different tin precursors at 10%(Sn/Sn+Cu)

As can be see here, since there is no significant Raman shift when we compared the spectrum of the film obtained using different precursors, thus they are subject to the same amount of stress in all the cases.

The tin (II) 2-ethylhexanoate is the one that shows the greatest intensity of the copper oxide peaks while the use of tin (II) acetate shows the smoother peaks and this can be linked with the different amount of incorporated tin in the film as will be shown in section 4.1.2.

The organic contaminations strongly vary with the used precursor and tin (II) acetate and tin (II) acac (liquid) show the highest content of these impurities.

In the tin (II) acac (liquid) case, it is possible to evidence a slight inclination of the Raman spectrum that can be due to some fluorescence, due to the presence of photoluminescence defects in the structure, as shown in (Mg/Mg+Cu) explained in Resende[1].

This phenomenon is also present in the lithium doped copper oxide (Li/Li+Cu) case as presented in the section 5.1 of this Master thesis.

Further investigations are necessary to understand better how the deposition conditions can influence the structural properties of the film and how the different amounts of tin incorporation can modify the intensity of the peaks and the organic contaminations.

4.1.2 Morphological characteristics

Figure 4.2 shows the effect of the different tin precursors on the surface. These SEM picture were obtained with a magnification of 20 000X.

It is noticeable that, although the concentration of tin in the initial solution is the same, the effect on the surface is different. The shown surfaces has been deposited with the deposition conditions written in the introduction of this paragraph. For the tin (II) acac (liquid) and for the tin (II) 2-ethylhexanoate, the surface shows a granular structure and these two precursors leads to the formation of grains with comparable size.

As shown next, these two precursors also lead an incorporation of the tin in the film between 1.5% and 2%.

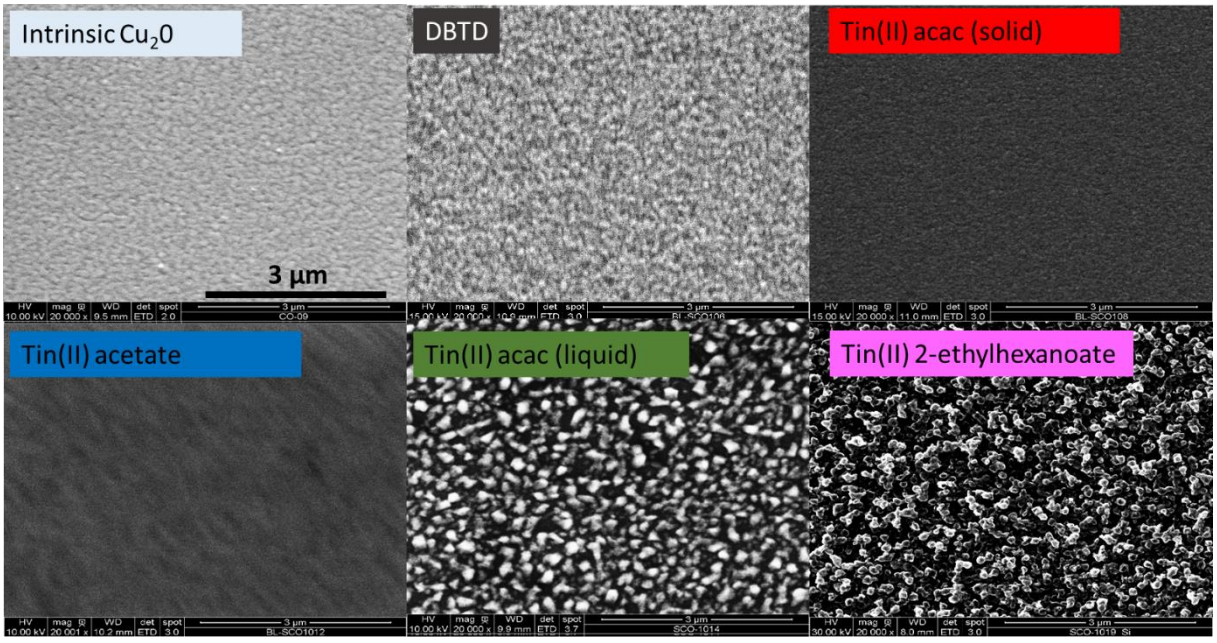

Figure 4.2 SEM imaging for the different tin precursors at 10% (Sn/Sn+Cu). The used magnification is 20000X

A comparison between the intrinsic case and the doping with DBTD and tin(II) acac (solid) leads to assert that the surface modifications are not so evident in these cases, showing a uniform structure with quite small grain size. The morphology is similar for all films except for tin (II) acac (liquid) where the film does not cover completely the glass substrate and for tin (II) 2-ethylhexanoate where the films exhibits porous structure with a high roughness. For the differences in morphology, the incorporation level of the different dopant should be taken in account. Further considerations and characterizations are necessaries in this framework taking in account also the different thicknesses of the samples.

In the table 3, the contents of tin incorporated in the film for the different tin precursors is presented, these are obtained through the use of EDS characterization, reminding that the initial concentration in the solution is kept fixed to 10%(Sn/Sn+Cu). These measurements have been performed with an energy source of 10KeV.

Table 3 Tin oxidation state in the used precursors and amount found in the film through EDS characterization of the 10% (Sn/Sn+Cu) case

Name	Oxidation state in the solution	Tin amount in the film (%)	Net XPS count/s Sn 10^4	Net XPS count/s Cu 10^4
DBTD	**+4**	**10.9**	**4**	**15**
Tin(II) acetylacetonate(solid)	**+2**	**0.1**		
Tin(II) Acetate	**+2**	**0**		
Tin(II) acetylacetonate(liquid)	**+2**	**1.4**	**1.2**	**23**
Tin(II) 2-ethylhexanoate	**+2**	**2**	**0.06**	**22**

As shown here, the incorporation takes place mainly with the doping with DBTD, with a measured content higher than the one in the solution.

The samples where tin(II) acac (liquid) and tin(II) 2-ethylhexanoate are used as precursors show a non-null amount of tin in the film, while for the others precursors, tin(II) acetylacetonate (solid) and tin(II) Acetate, the measured content in the layer is practically null.

Moreover, further investigations are necessaries to understand better this phenomena and the tin's oxidation state in the film, starting from the one in the precursor, listed in table.

In this research framework, XPS measurement were performed comparing the effect of the DBTD and the tin (II) acetylacetonate (liquid) on the oxidation state of tin in the film.
As shown in figure 4.3, the XPS spectrum present the different binding energy of the formed compound and these energies where compared with the one found in literature as in in Jie[39] for the different tin compounds. Stannic and stannous oxide have a binding energy of 486.80 eV and 487.16 eV respectively, characteristic of the $3d_{5/2}$ orbital, and their difference is 0,36 eV.

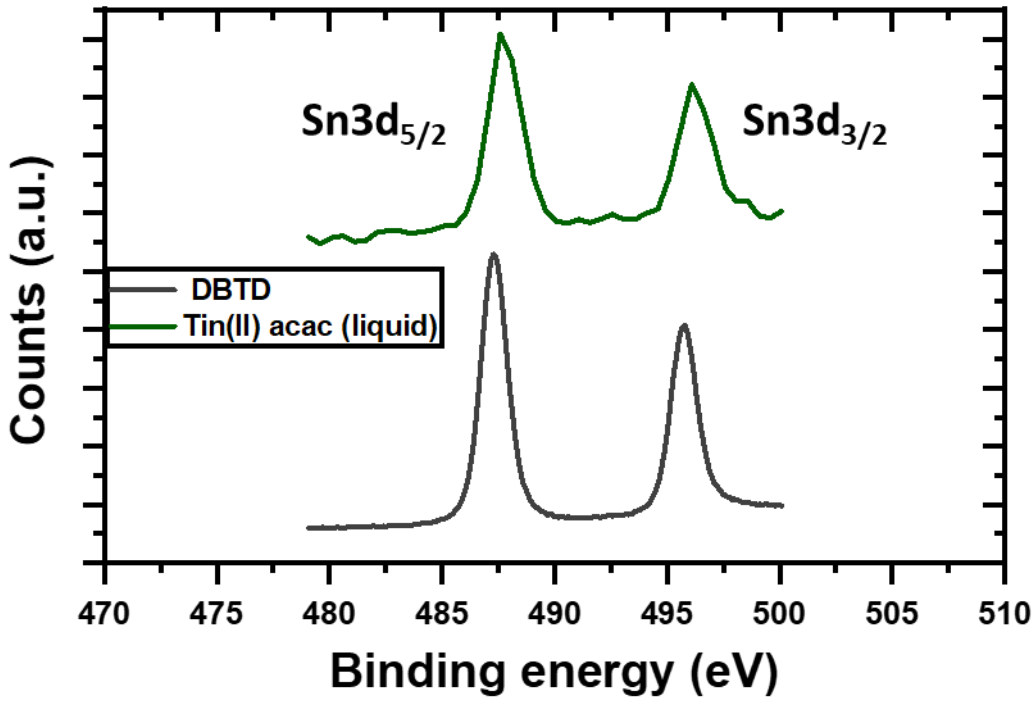

Figure 4.3 XPS measurement for tin 3d orbitals for a sample 10%(Sn/Sn+Cu) of DBTD compared with the 10%(Sn/Sn+Cu) with tin(II) acac (liquid) as precursors.

In this case, it is possible to assert that the XPS spectrum of the tin (II) acac (liquid) present sharper peaks and the measurement is subject to more electronic noise.

DBTD and tin (II) acac (liquid) have tin oxidation state equal to +4 and +2 respectively in the initial solution. From this graph, it is possible to evidence that a slight peaks' shift is shown but the difference between these two cases is not enough to be related with the change in the oxidation state of the dopant. According to literature, the energy shift between the +2 and +4 oxidation state is very small and cannot be detected with the used characterization tool. For these measurements, further investigations are necessaries.

4.1.3 Electrical properties

As pictured in figure 4.2, the incorporation of the tin could have an impact on the morphology and as presented in figure 4.4 could modify the electrical properties of the film.

In this plot, there is the comparison of the values of sheet resistance of the as deposited samples for the used deposition temperature, 325°C and 350°C.

From figure 4.4, it is noticeable that there is an improvement of the conductivity with respect to the intrinsic copper oxide case using a lower deposition temperature and DBTD or tin (II) acac (liquid) as precursors, reaching values around 20MΩ/sq, close to the intrinsic case, and 10MΩ/sq respectively.

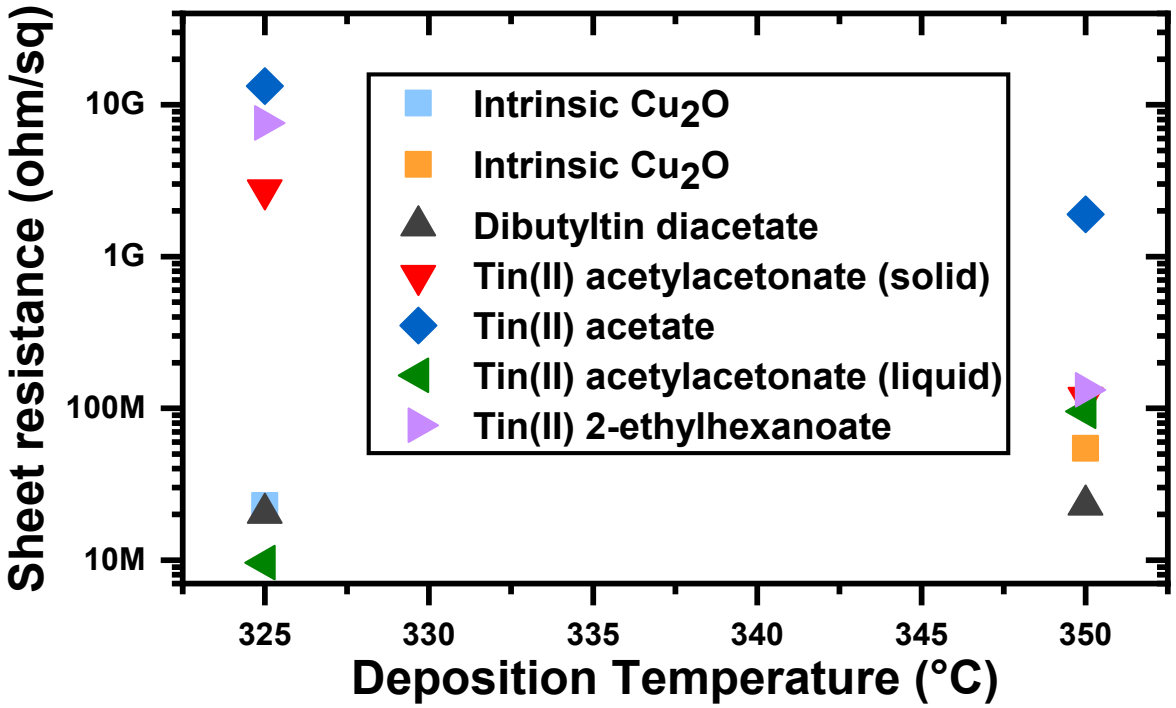

Figure 4.4 Sheet resistance values for the two different deposition temperatures for the used different precursors in the 10% (Sn/Sn+Cu) case.

The tin (II) acetylacetonate (liquid) improve the conduction for a deposition temperature equal to 325°C, with a sheet resistance value of 9.1 MΩ/sq, while when it is deposited at 350°C its sheet resistance increases of one order of magnitude. Furthermore, the incorporation of the dopant takes place also in the tin (II) 2-ethylhexanoate but this precursor does not show an improvement of the conduction. This fact can be related to the non-continuous morphology as evidenced by SEM imaging while in the case of tin (II) acetate the low conductivity can be linked to the high organic contaminations, as proved by Raman spectroscopy. Moreover the thickness of the samples should be taken in account.

The others precursors are not incorporated in the film and they do not enhance the electrical properties of the film with these deposition conditions. As conclusion, it is possible to assert that an incorporation of the tin as dopant can be used to obtain an enhancement of the electrical properties depending by the deposition conditions.

From these results, an enhancement of the electrical properties is obtained and this arises new questions about the charge carrier in this material, establishing if it is an n-type semiconductor or a p-type one. This lead the necessity to perform more analyses to understand better how these precursors influence the performance of the film.

4.1.4 Optical properties

In figure 4.5, it is possible to investigate the effect of the different precursors on the transmittance spectrum with the deposition conditions listed in the legend. We should keep in mind that further investigations on the thickness of the samples are necessary but qualitatively, is possible to notice

that the samples with the tin(II) acetylacetonate (solid) has not sufficient thickness to have refraction. In these cases, generally the deposited thickness will be between 40nm and 200nm as demonstrated by the fact that we have only one refraction peak. Moreover, as evidenced by these spectrum in the IR range, the tin(II) acetylacetonate (liquid) and the tin(II) 2-ethylhexanoate show a thickness comparable with the intrinsic case deposited at 325°C with a precursor rate of 0,015mmol/min.

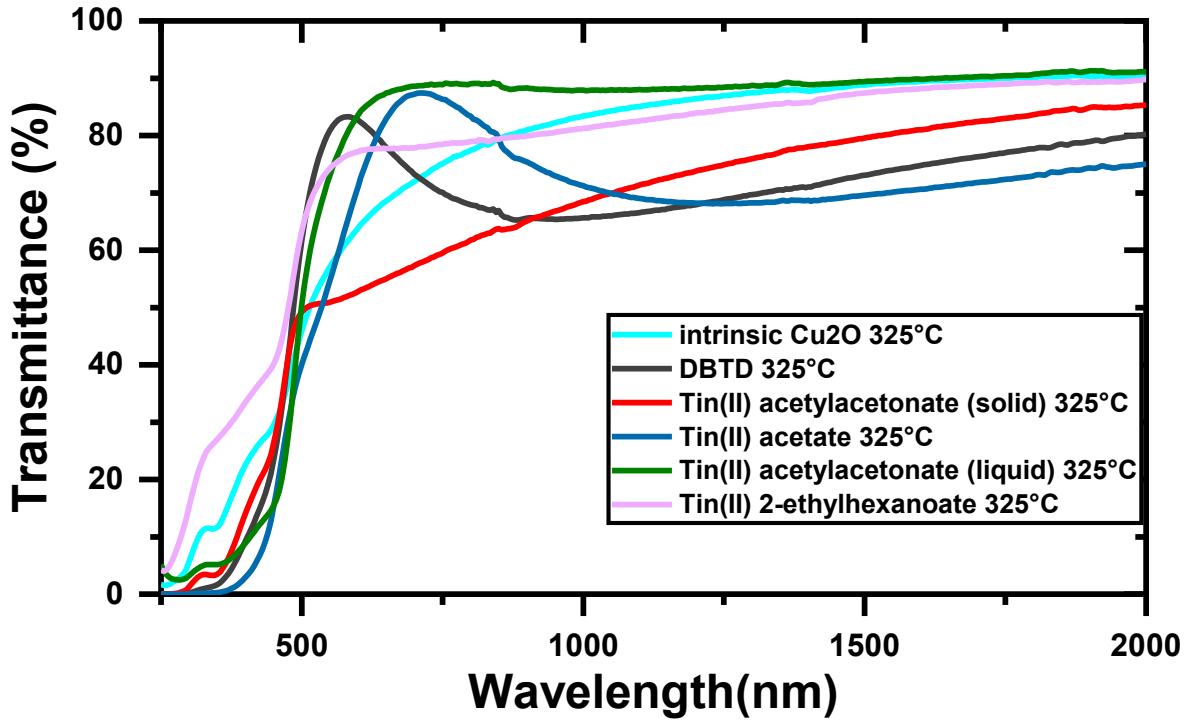

Figure 4.5 Transmittance spectrum of the listed used tin precursors with a solution concentration of 10%(Sn/Sn+Cu)

Additionally, while the others precursors show a peaked spectrum, tin (II) acetylacetonate (liquid) and tin (II) 2-ethylhexanoate have a quite flat spectrums. The high transmittance of the tin (II) 2-ethylhexanoate at 300nm could be attributed to the non-continuous morphology shown from the sample. Comparing the intrinsic case with the use of tin as dopant, there is a general improvement of the optical performances but further measurements of the thickness are necessaries.

The link between the optical and the electrical properties is shown in figure 4.6. As already shown, the best sheet resistance values are obtained for the tin (II) acac (liquid) but it shows a slight reduction of the average transmittance in the visible range, reaching values around 57%, with respect to the DBTD's case, which measures an average transmittance around 59%.

As possible to notice in the following graph, figure 4.6, tin (II) 2-ethylhexanoate shows good optical properties but it has one of the worst electrical properties for these deposition conditions.

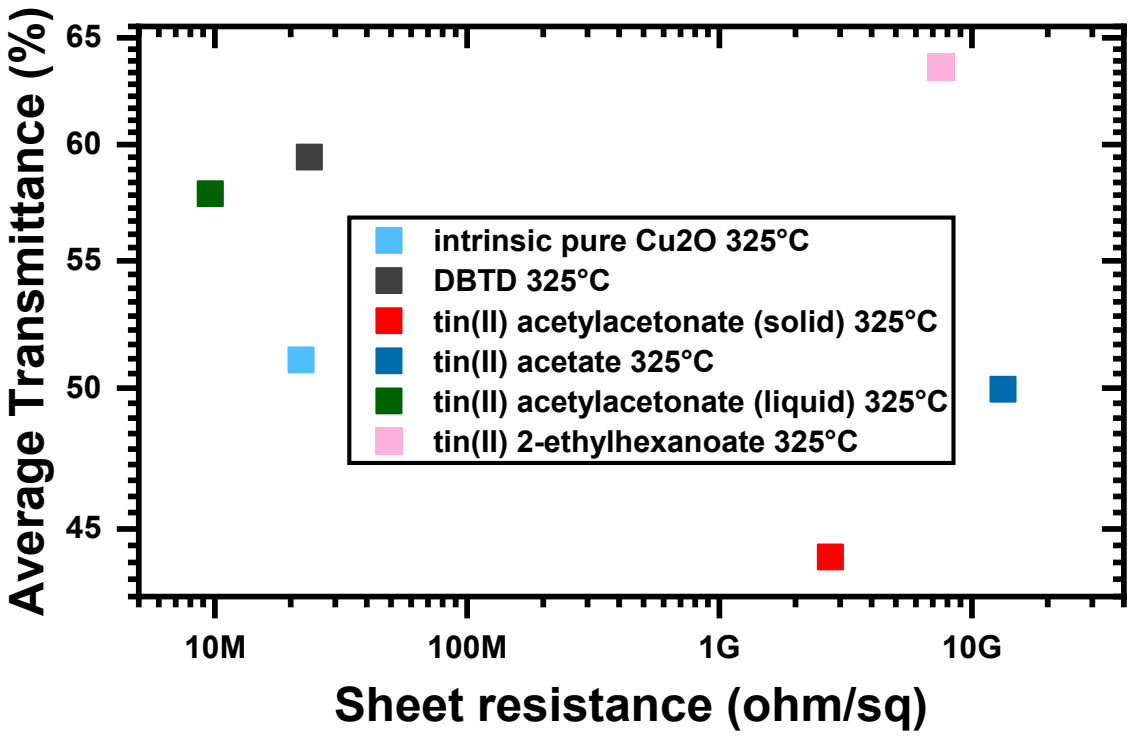

Figure 4.6 Average Transmittance versus the sheet resistance values for the different precursors at 10%(Sn/Sn+Cu)

In this case, it is shown how tin doping can help the conduction and the transmittance based on the different chemical precursors. DBTD, the tin (II) acac (liquid) and tin(II) 2-ethylhexanoate are incorporated in the film and they improve the optical transmittance with respect to the intrinsic case. Moreover, the best properties for this research are obtained for the tin (II) acac (liquid) which shown better optical and electrical properties. Further investigations are necessaries to link these properties with the thickness of the samples and to discover the type of carrier responsible of the conduction in these materials.

4.1.5 Thermal treatment

In this paragraph, there will be the study of the effect of the thermal treatment for different tin precursors used. The results are shown only for some of the studied organotin precursors, for major clarity.

Furthermore, as explained in Musa[41] in the case of chlorine doping and annealing can lead to an enhanced mobility of the samples.

In figure 4,7, the annealing curves are shown. As explained in chapter III, it is the plot of the resistance plotted against the inverse of the temperature in Kelvin degrees.

In this case, the annealed samples were deposited with a temperature of 350°C and a precursor rate of 0,015mmol/min and they experienced a thermal treatment with a maximum temperature of 250°C for 1 hour.

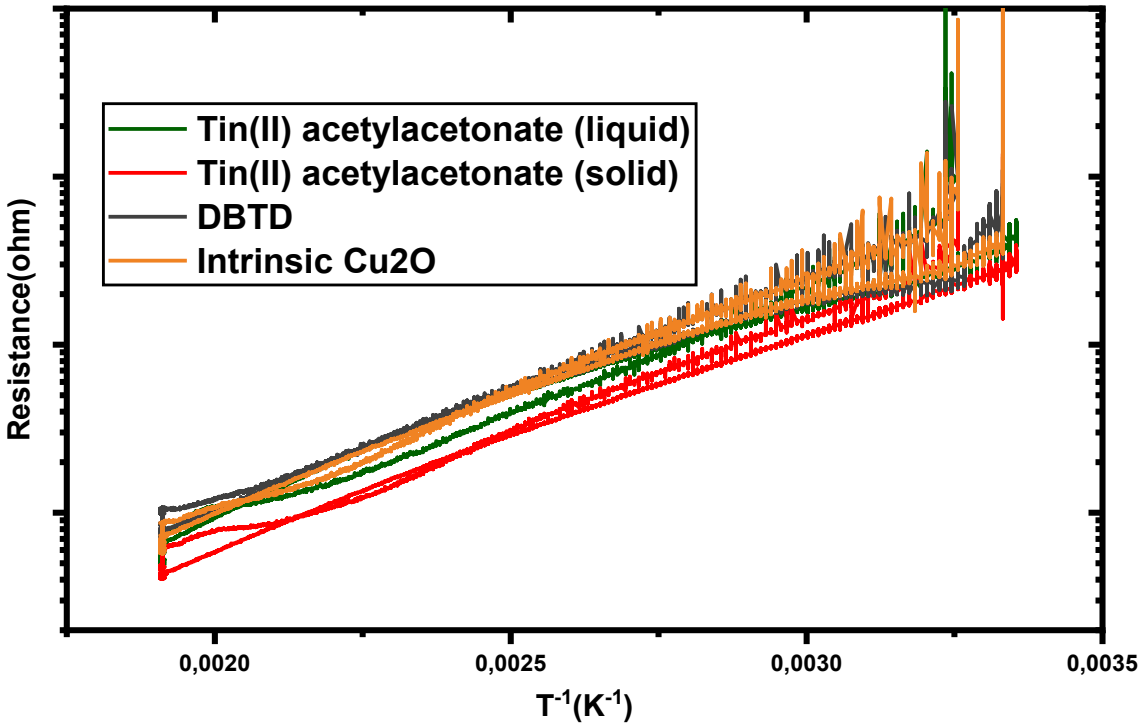

Figure 4.7 Resistance variation during the thermal annealing for the listed used tin precursors with a solution concentration of 10%(Sn/Sn+Cu)

As shown from this graph, the curves present in all the cases a reduction of the sheet resistance with the thermal treatment and the initial and final values of this parameter are reported in the table 4.

In the table 4, the calculated values of the activation energies are reported. The activation energy is calculated, as in the case of pure copper oxide, from the slope of these curves during the cooling down. In this case in the temperature range of 180°C down to 170°C, where the curves presented a more linear slope.

Table 4 Initial and final sheet resistance and respective activation energies for the different studied tin precursors

Sample	Initial Sheet resistance (Mohm/sq)	Final Sheet resistance (Mohm/sq)	Activation energy (meV)
tin(II) acetylacetonate (solid)	44.7	33.2	288,05
tin(II) acetylacetonate (liquid)	89.9	56.6	277,19
DBTD	23.6	14.9	271,37
Pure Cu_2O	47	31	275.72

As it is possible to see from these values, the activation energies are similar to the one of the intrinsic cuprous oxide and a reduction of the sheet resistance always occurred. This should also

be linked with the different amount of tin incorporated in the film, keeping in mind that tin (II) acetylacetonate (solid) does not lead to an incorporation of the dopant.

Further studies are necessaries to understand better how the different precursors react under thermal treatment and how parameters as temperature and time should be modified to obtain a greater enhancement of the electrical properties of the film.

Moreover, others analyses have to be performed to understand how the vacancies can be activated through the thermal treatment and if a change in phase occurs.

4.2 Tin doped copper oxide results with Dibutyltin Diacetate as Precursor

The tin doping through this precursor is justified by the already known use to deposit thin film of tin oxide as shown in Melsheir[86], Fan[87], Nelli[88], Mannie[89] and Ashida[90]. This chemical organotin precursor is also well-known for the possibility to be used as tin precursor in doped system for tin oxide as in the case of antimony doping for solar cell applications[91], for the doping with europium as shown in Fan[87], fluorine as in the case of Hanif[92] and platinum as in Tadeev[93]. Moreover, it is been proved that this material can be used as precursor to dope oxides with tin, as shown in Canevali[94] and Chiodini[95] for Si_2O and as demonstrated by Pabchanda[96] for the zinc oxide case.

4.2.1 Structural properties

Figure 4.8 shows the Raman spectrums for the different amount of DBTD in the solution, which are indicated by the percentages listed on the side. A comparison with pure copper oxide spectrum is done to evidence the main differences. In this case, not all the deposited samples are shown for major clarity. These samples were deposited with a deposition temperature of 350°C and a precursor rate of 0,015mmol/min with duration of the deposition of 1 hour.

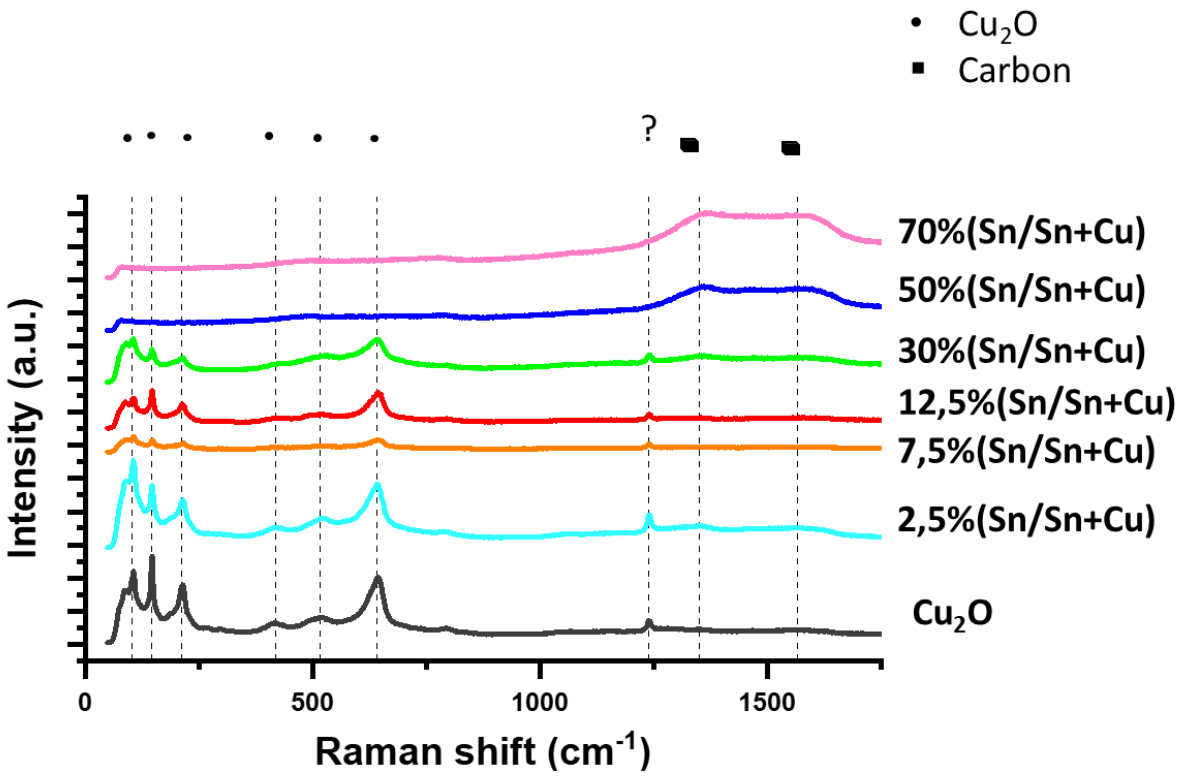

Figure 4.8 Raman spectroscopy of (Sn/Sn+Cu) for different amount of DBTD in the solution.

The peaks, of the cuprous phase, at lower Raman shift, are in the same position as the intrinsic material and their intensity reduces with an higher amount of tin in the solution up to almost disappear for the cases where the doping is equal or higher 50%(Sn/Sn+Cu). It is also possible to notice that this reduction is not strictly dependent by the amount of tin in the solution as evidenced by the 7.5%(Sn/Sn+Cu) case. The unknown peak follows the same behaviour of the others ones, disappearing in the 50%(Sn/Sn+Cu) and the 70%(Sn/Sn+Cu) cases.

This could be related to an amorphous compound obtained between Cu_20 and SnO_2 justified by the disappearing of the cuprous oxide related peaks for these doping levels. It is also possible to notice that, since no significant Raman shift is present, the different amount of tin used in the solution provoke the same amount of stress in the films.

Moreover the organic contaminations are relevant for the 50%(Sn/Sn+Cu) and for the 70%(Sn/Sn+Cu) cases, while in the others cases they are limited. A slight increase of these compounds can be seen in the 2.5%(Sn/Sn+Cu) case.

4.2.2 Morphological characteristics

In figure 4.9, it is possible to visualize the SEM images of the surfaces of the tin doped cuprous oxide with DBTD as precursor. These images were obtained by the analysis of the secondary electron signal with a magnification equal to 50000X.

Only some of the doping levels are shown, obtained with the same deposition conditions with a temperature equal to 325°C and a precursor rate of 0,015mmol/min always with a deposition time of one hour.

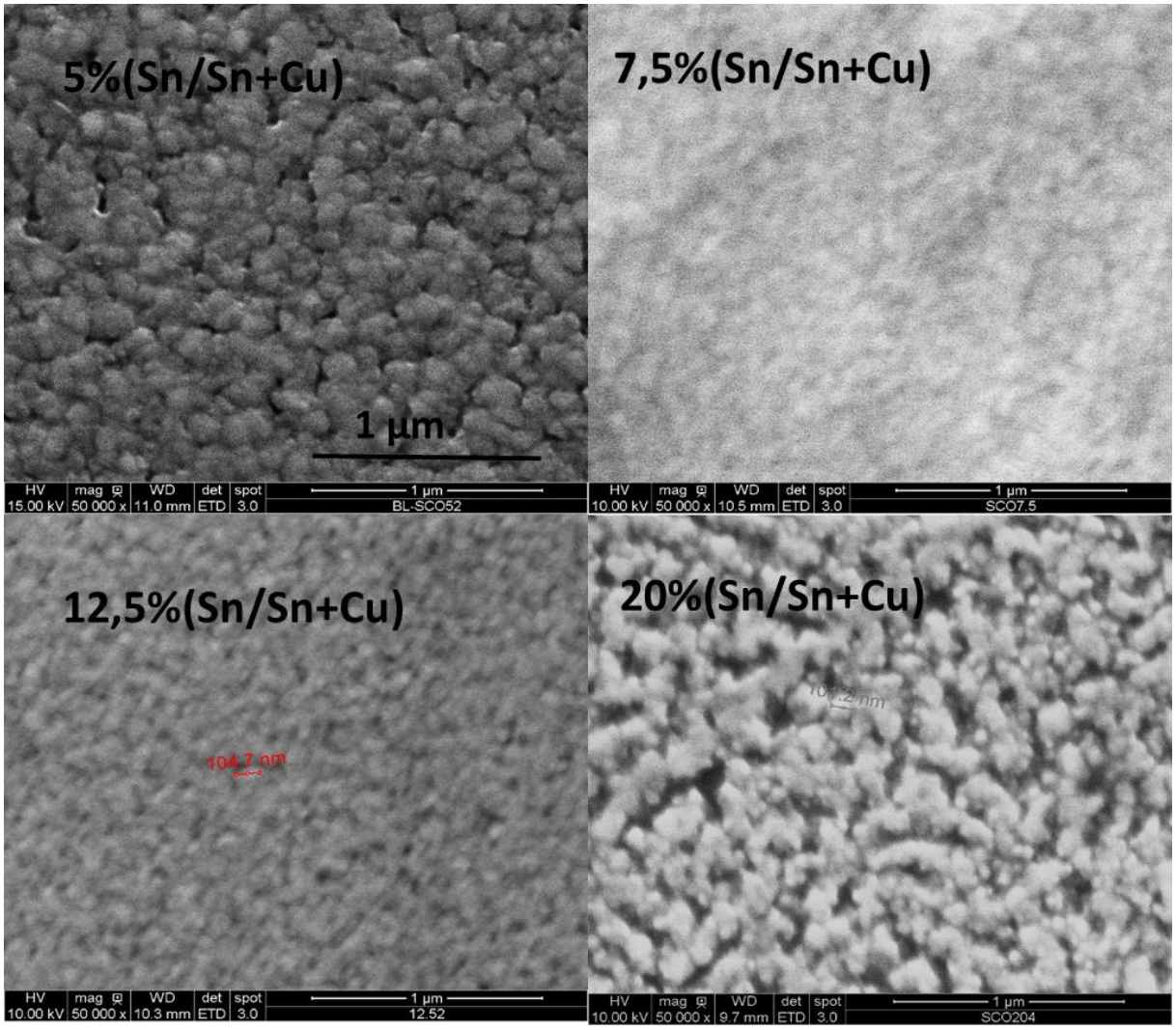

Figure 4.9 SEM imaging of (Sn/Sn+Cu) for different amount of DBTD with a magnification of 50000X

The effect of the doping level modifies the surface, showing different results and especially, 5%(Sn/Sn+Cu) and 20%(Sn/Sn+Cu) samples show the most irregular structure with well-defined grains. Moreover, these two last cases show a not complete deposition with surfaces with holes, mainly visible in the 20%(Sn/Sn+Cu) case. The not complete formation of the film, as testify by this SEM image, could lead to the higher value of sheet resistance as presented in the section 4.2.3 but in this case the deposition temperature was equal to 350°C, thus further investigations are required.

The others two surfaces, instead, show a more regular surface with less defined grains boundaries with respect to the previous cases. This can be justified from the different incorporation level of the dopant of the film as shown in figure 4.10, but further investigations are necessaries. Moreover,

others analyses about the thickness of the samples are required to connect the topological properties of the films with the different crystal growth and how this is related to the formation of the grains and their size.

In figure 4.10, WDS is been used to measure the amount of dopant is incorporated in the deposited films knowing the tin solution concentration. These measurements were performed in three different point of the samples and the presented results are the mathematical average of these.

The presented samples has been deposited with a temperature of 350°C and a precursor rate of 0,015mmol/min. The results of this technique are obtained by fitting with the Stratagem software the data measured with three different probing energies (11, 16, 22KeV) determining the volume of interaction of the imping beam. For this reason, they are related with the measured amount of tin in the film and its thickness.

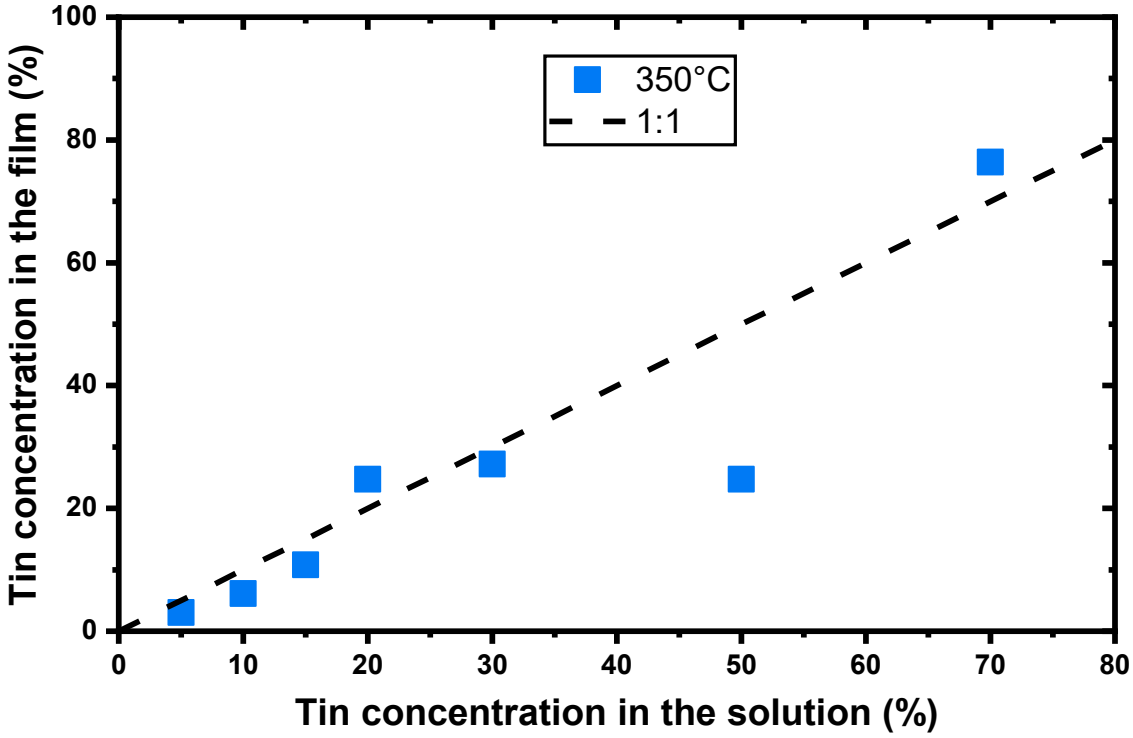

Figure 4.10 WDS quantification for the different amount of tin in the film with DBTD as precursor.

In this plot, it is noticeable how the amount of tin in the film is generally slightly lower than the 1:1 ratio, shown as the dashed line. As it possible to evidence here, the depositions successfully incorporate the tin in the film in different amount based on the initial tin concentration in the solution.

From this graph, it is also relevant how the incorporation in the films is almost linear for level lower than 30%(Sn/Sn+Cu) case of tin doping, using DBTD as precursor.

Moreover, as it is possible to understand from the comparison between figure 4.10 and the amount of tin in film obtained by EDS shown in table 3, a higher deposition temperature leads to a

decreased amount of dopant in the film. Indeed, when the used deposition temperature was 325°C, the amount of tin found in the layer is equal to 10.9% greater than in the case deposited at 350°C.

Demonstrated the incorporation of the tin in the layer using DBTD as organotin precursor, a XPS measurement was performed to measure the binding energy and to deduct the oxidation state of the dopant in the film. These energies were compared with the ones found in literature as in Jie[39] for the different tin compounds. Stannic and stannous oxide have a binding energy of 486.80 eV and 487.16 eV respectively, characteristic of the $3d_{5/2}$ orbital,, and their difference is around 0,30 eV.

In figure 4.11 is shown the XPS spectrum for the 3d orbitals of the 10%(Sn/Sn+Cu) case with DTDB as precursor deposited at 325°C with a precursor rate of 0,015mmol/min for a total deposition duration of one hour.

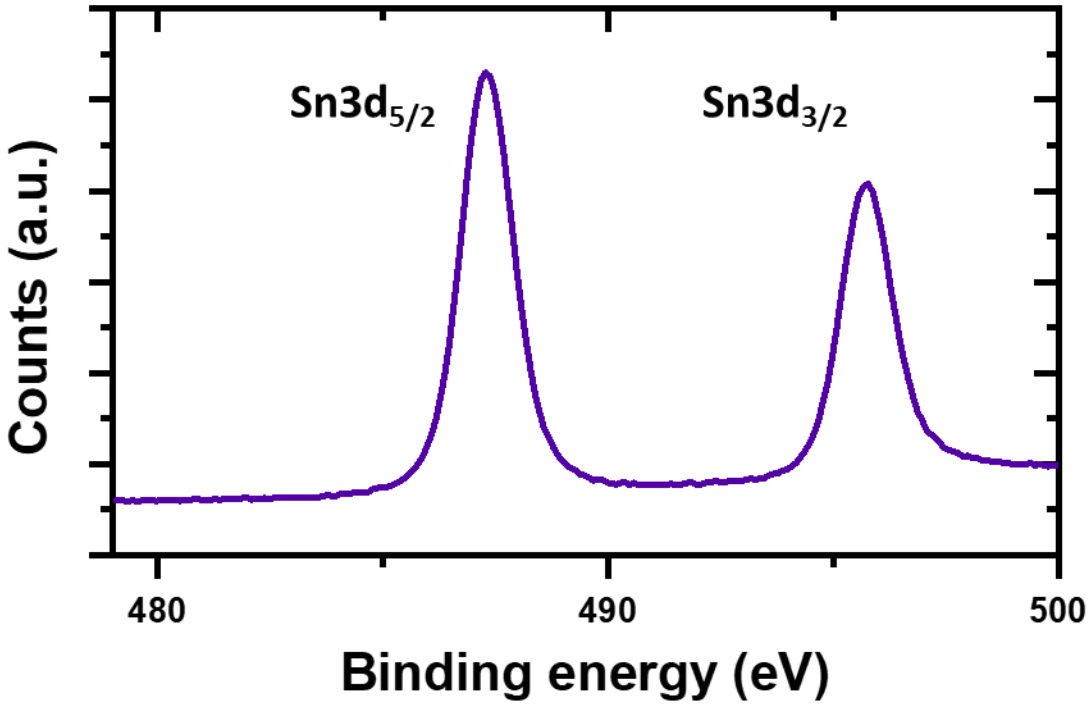

Figure 4.11 XPS measurement for tin 3d orbitals for a sample 10%(Sn/Sn+Cu) of DBTD deposited at 325°C with a precursor rate of 0,015mmol/min.

From this spectrum in figure 4.11 it is clear the presence of tin compound revealed by the peak around 487, 5 eV characteristic of the $3d_{5/2}$ orbital, but, since their very low difference in binding energy, the sensitivity of the measurement apparatus is not enough to determine precisely the tin oxidation state.

Another way to evaluate the oxidation state of the element is based on the study of the Auger peak, but in the tin case the intensity was too small to obtain useful information.

4.2.3 Electrical properties

The widest study on the tin incorporation effect in the film was performed on DBDT and the electrical properties obtained with such precursor are shown in figure 4.12. The plot shows the sheet resistance variation for different amount of doping for the deposition at 350°C and precursor rate of 0,015mmol/min. It is clear that the tin doping has an effect on the electrical properties of the film and furthermore for tin's concentration lower than the 20%(Sn/Sn+Cu) in the original solution, the behaviour is almost parabolic with a minimum around the 10%(Sn/Sn+Cu).

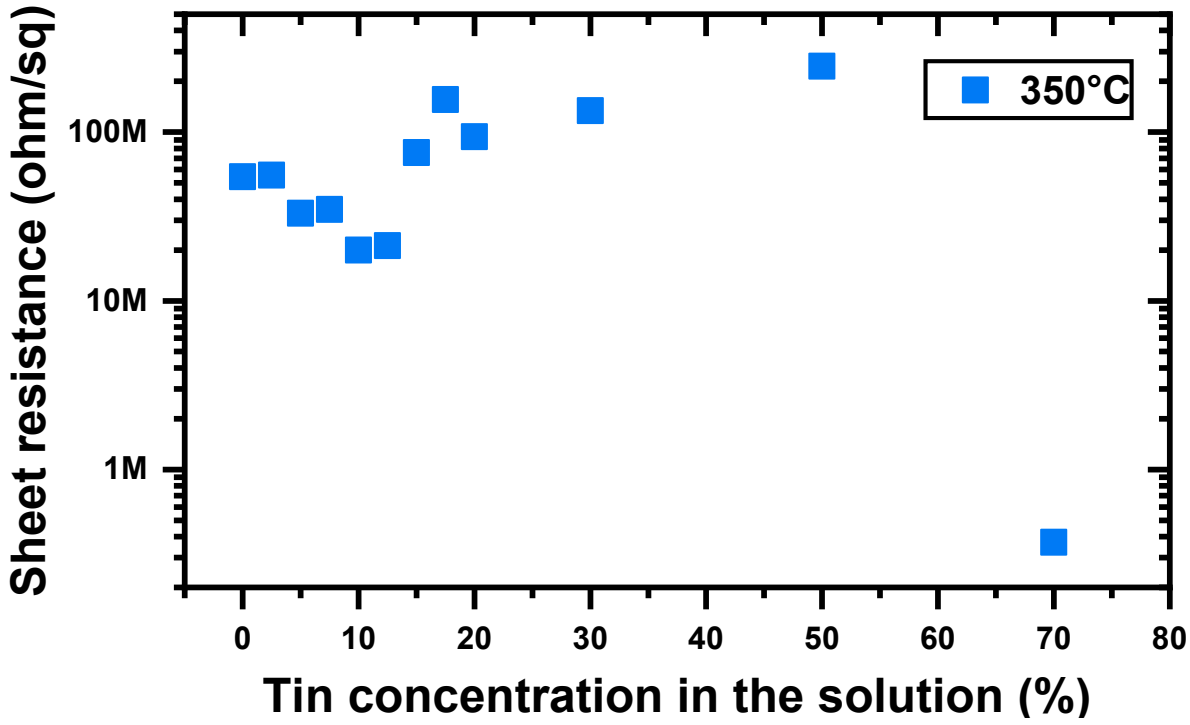

Figure 4.12 Sheet resistance of the (Sn/Sn+Cu) for the different amount of DBTD in the solution

When the doping with tin overcome the 50%(Sn/Sn+Cu), there a drastic drop of the sheet resistance and this will also show very good optical properties, as will be presented in the following section, but this material is characterized by the fact it is a n-type semiconductor, SnO_2, as reported in Trypathy[35].

Since the interest of this research, these results show a minimum of the sheet resistance for the 10%(Sn/Sn+Cu) case.

4.2.4 Optical properties

Transmittance measurement were performed to evaluate the effect of the different amount of DBTD in the initial solution, deposited with the conditions listed before, on the optical properties.

As possible see in figure 4.13, the 50%(Sn/Sn+Cu) show a very highest transmittance being almost transparent macroscopically as well as the 70%(Sn/Sn+Cu) case.

Moreover the comparison between the 30%(Sn/Sn+Cu) case and the 2.5%(Sn/Sn+Cu) case shows that an increase of the doping slightly improve the optical properties but this has to be related to different thickness of the samples. As main range, the achieved thickness is limited demonstrated by the fact that the show one refraction peak in the transmittance spectrum.

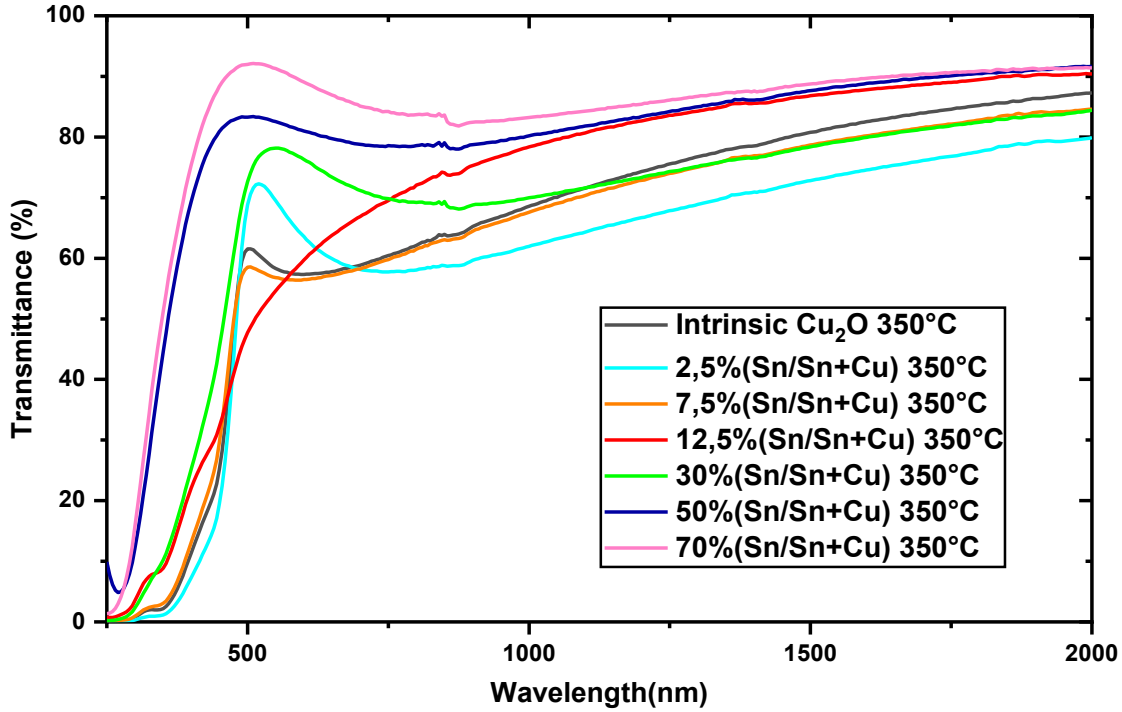

Figure 4.13 Transmittance spectrums for different percentage of DBTD in the solution.

In deed as shown from the cases 7.5%(Sn/Sn+Cu) and 12,5%(Sn/Sn+Cu) an increasing doping level does not directly means an improvement of the transmittance in the visible. This effect is clearly related to the different obtained thickness due to the fact that the 12,5%(Sn/Sn+Cu) sample is so thin that it does not present interference peak. Moreover, the intrinsic case spectrum is very similar to the doped case of 7.5%(Sn/Sn+Cu) and the difference can be attributed to the lower thickness of the intrinsic sample.

Further studies have to be perform in order to understand better how the different percentages of tin precursor in the solution influence the thickness and the optical properties of the samples.

In the plots in figure 4.14 a) there is the average transmittance in the visible range (390nm-700nm) plotted versus the different amount of DBDT deposited at 350°C with a total precursor rate of 0,015mmol/min. Figure4.14 b) shows the link between optical and electrical properties.

As it is possible to notice from figure 4.14a), there is a slight improvement, around 10%, of the average transmittance with respect to the intrinsic case when the doping overcome 10%(Sn/Sn+Cu) but this is not true for all the greater percentage.

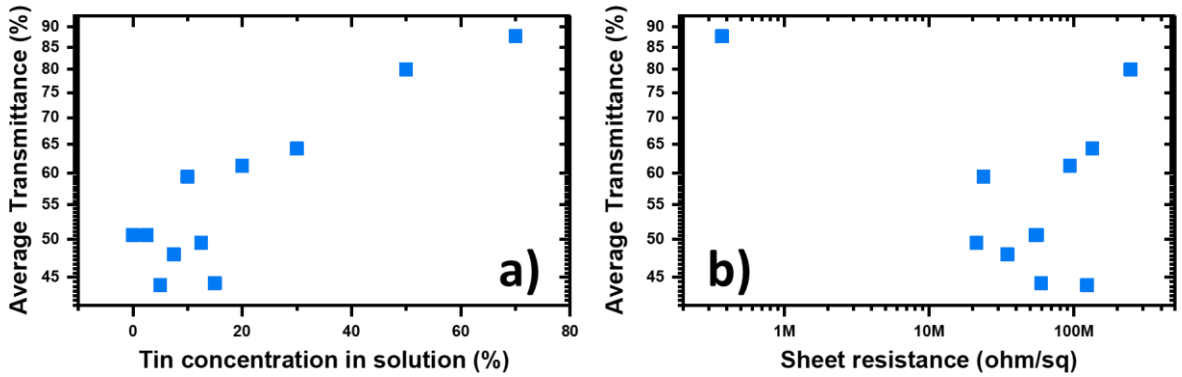

Figure 4.14 a) Average transmittance versus tin amount in the solution b) Average transmittance versus sheet resistance

In figure 4.14b) instead, the values around 20 MΩ are obtained for 10%(Sn/Sn+Cu) and 12.5%(Sn/Sn+Cu) samples. The 10%(Sn/Sn+Cu) is the only one improving both electricals and optical properties when compared with the intrinsic case deposited in the same conditions. Indeed, the intrinsic case in these deposition conditions shows a sheet resistance of around 50 MΩ/sq and an average transmittance of 49%.

Further investigation are necessaries, to understand better the role of this precursor and of the deposition conditions on the film growth and its thickness. Moreover, from the electrical point of view, others measurements about the charge carriers and their concentration are required.

4.2.5 Thermal treatment

As shown in figure 4.15, a thermal annealing in the open atmosphere were performed the samples with different amount of tin doping in the initial solution, listed in the legend. The temperature was kept constant, as for the others cases, to 250°C for 1 hour. These samples were deposited with a temperature of 325°C and a precursor rate of 0,015mmol/min. In this section not the totality annealed samples are shown for major clarity. The graph shows also a comparison with the intrinsic case deposited in the same conditions.

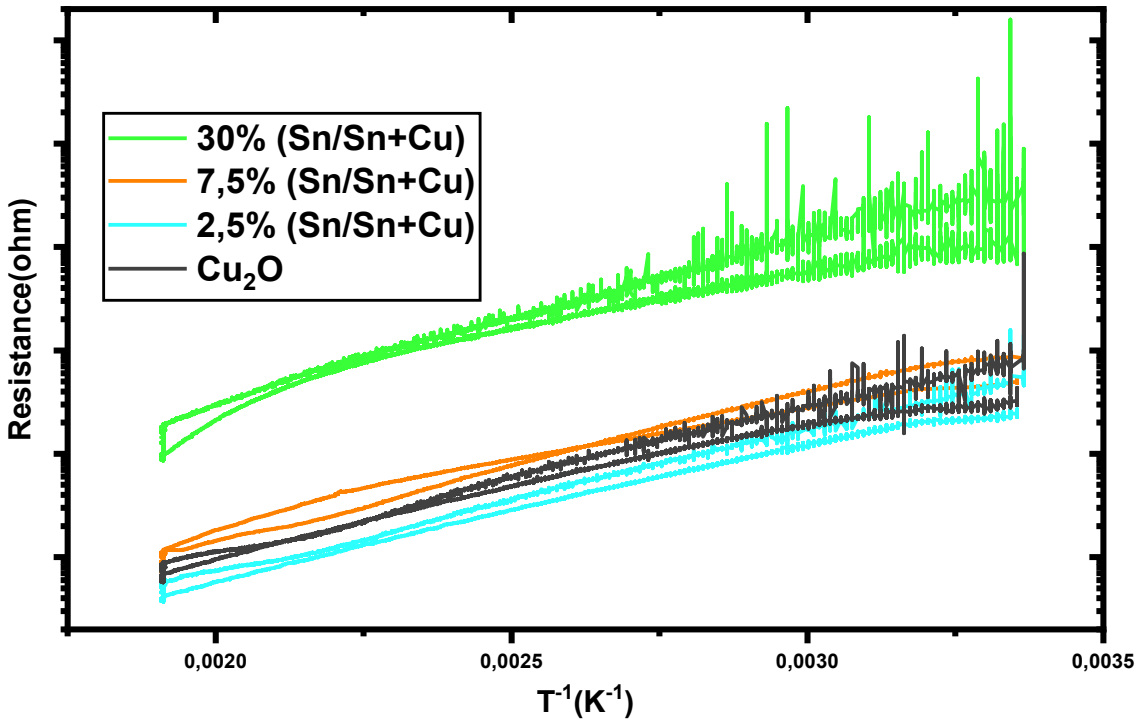

Figure 4.15 Resistance variation during the thermal annealing for the listed DBTD molar concentration in the initial solution

As it is noticeable from figure 4.15, there is a general reduction of the resistance after the thermal treatment, as remarked from the values reported in the table 5.

Moreover, it is possible to evidence that in the case of 30%(Sn/Sn+Cu) and 7,5%(Sn/Sn+Cu) the cooling down present a more rounded shape with respect to the others cases and this should be taken in account during the calculation of the activation energy. From these curves is also clear that in any sample the thermal treatment could enhance the electrical properties justified by the fact that the final values of sheet resistance are always lower than the initial ones except in the 30%(Sn/Sn+Cu) case as summarized in the next table.

These values, shown in table 5, are calculated with a linear fit of the curve during the cooling down, specifically from 120° C down to 110°C where the curves present a more regular shape.

Table 5 Initial and final sheet resistance and respective activation energies for the different amount of DBTD

Sample	Initial Sheet resistance (Mohm/sq)	Final Sheet resistance (Mohm/sq)	Activation energy (meV)
30%(Sn/Sn+Cu)	2250	2280	234,4
7,5%(Sn/Sn+Cu)	67.1	34.1	205,15
2,5%(Sn/Sn+Cu)	37.2	24.4	258,79
Pure Cu_2O	34	35	275.72

The effect of the thermal treatment clearly correspond to a reduction of the sheet resistance except in the case where the highest concentration of DBTD in the solution is used.

As it is possible to notice from these values, the tin doping generally leads to a reduction of the activation energy compared with the intrinsic case. Moreover, further studies on the effect of the thermal treatment have to be performed in order to understand better how the different amount of DBTD in the solution can influence this parameter. Indeed, from these values it is possible to notice that there is not a trend, changing the doping level.

5. Lithium doped cuprous oxide (Li/Li+Cu)

Lithium doped and precursor

Lithium is a chemical element with symbol Li and atomic number 3. It is a soft, silvery-white alkali metal. In this research framework, the main purpose was to study the possibility to create CuLiO phase, for this reason the used percentage of lithium in the initial solution was greater than the tin case. This compound can be used as possible p-type transparent oxide semiconductor as explained in Yim[97]. Many others studies are related to the analysis of the lithium-copper phase as in Saito[98], especially as dopant in the case of copper oxide as shown in Priscilla[6] and Kim[99].

Within compounds, Lithium is used in many applications as ceramic and glass, lithium batteries, Li-ion batteries. The doping of different materials with lithium is already known in literature and used in different application as in batteries[100], capacitors[101] and Metal Organic Framework for H_2 storage[102]. Moreover, this material is already been studied forming different compounds and used as temperature sensor[103] , moreover, in literature there are many articles describing the possibility to use copper oxide as anode for lithium battery as reported in Iijima[104] and in Thi[105].

This material is known as dopant for different oxide as SnO_2[106], NiO[107], MgO[108], ZnO[109], TiO_2[110] and also as co-dopant with Gallium in the case of NiO[111].

Within this master thesis as exploratory experiments there is the study of the possibility to deposit by aerosol assisted MOCVD mixed compound between Li, Cu and O.

In this study case, the used lithium precursor was the Li (II) acetylacetonate, briefly called Li (II) acac, always mixed with the copper precursor, Cu (II) acac. The depositions took place with 2 different amount of lithium in the solution (50%, 66%) and each percentage is been obtained using two different deposition temperatures. In the 50%(Li/Li+Cu) case the deposition took place at 300°C and 350°C, in the 66%(Li/Li+Cu) case the tested deposition temperatures were 350°C and 400°C.

During these depositions, the optimized deposition conditions for the pure copper oxide have been used, with a precursor rate equal to 0,015mmol/min. The deposition were performed with the same oxidizing environment of the previous cases with argon volume of 6l/min and 1,5l/min of oxygen. The pressure used was kept constant to 2,5mmH_2O and the deposition was 1 hour long. The results will be presented in the relative part.

The purpose of this Master thesis is to improve the properties of the film with respect to the intrinsic case, mainly looking for an enhancement of the electrical and optical properties, as in the case of tin doping. This research is also aimed to understand how the use of this chemical precursor and this dopant can modify the morphology and the structural properties of the film.

This study case has been studied less deeply with respect to the tin doping case, which was the major candidate of this research framework.

Lithium doped copper oxide results

5.1 Structural properties

In this section, no EDS nor WDS measurements were performed since the very light nature of the element does not allow the quantification of the amount of lithium in the film. So the composition of the sample 66%(Li/Li+Cu) deposited at 400°C was analysed by XPS. Deposition of Cu and Li is obtained but, due to the chemical contaminations in the reaction chamber the samples contain also Sn.

The structural properties for these films, obtained through the Raman spectroscopy, are shown in figure 5.1. In this case the various deposition temperatures are listed beside the different doping level and the precursors rate was kept equal to 0,015mmol/min obtained from the optimization of the pure copper oxide depositions.

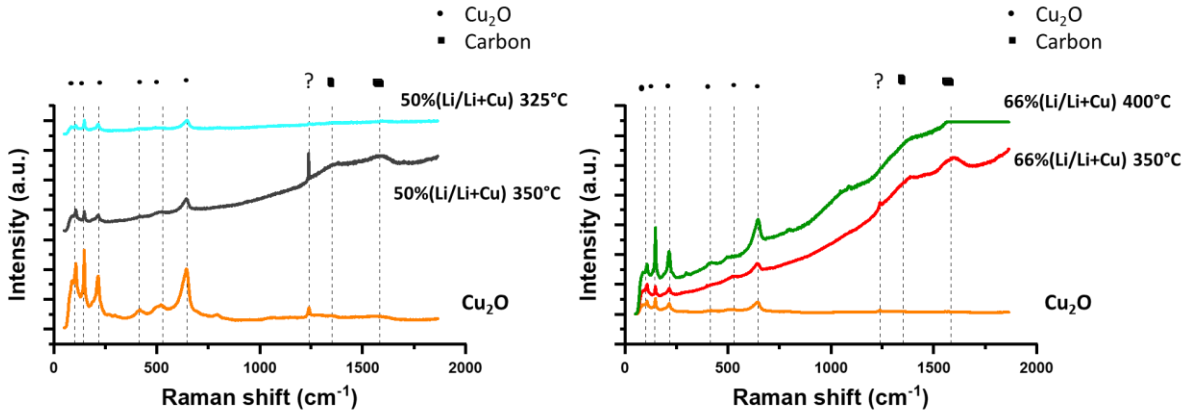

Figure 5.1 Raman spectrum for the lithium doped copper oxide (Li/Li+Cu)

In both the images of figure 5.1, both the Raman spectrum of the intrinsic case belong to the same sample. Comparing these intensities it is possible to notice that the 66%(Li/Li+Cu) case shows higher peaks' intensities. Moreover the 66%(Li/Li+Cu) case shows an increasing peaks' intensity when the deposition temperature is higher. For both the doping level, when the deposition temperature is set to 350°C or higher, there is a bending of the spectrums towards higher intensities. This could be related to fluorescence phenomena, resonance effect, which can be caused by very high organic contaminations or due to the presence of photoluminescence defects in the lattice. The huge intensity of this part of the Raman spectrums is due to the difference in energy between the incident photon and the one that reaches the sensor. In this case if photon generating defect are present, the amount of signal which contribute to the Raman lines is huge leading to this bending.

The main difference between the two 50%(Li/Li+Cu) samples is noticeable, indeed when a higher deposition temperature is used there is the bending of the Raman spectrum. This could prove that a lower deposition temperature does not allow the formation of such photoluminescence defects.

From these analyses, it is only possible to evidence the presence of Cu2O peaks but not lithium related ones, even if the thickness of these samples is very low as proved from the transmittance spectrum in the IR. For these reasons XRD measurement are necessaries to analyse the phase and XPS to quantify the amount of Li in the different films.

5.2 Morphological characteristics

For this material, the study of the surface was performed through SEM and the results are presented in figure 5.3. A magnification level of 20.000X was used with the detection of secondary electron to perform the imaging. As already explained in the introduction of this chapter no EDS characterization were possible due to the very low atomic number of the lithium. Furthermore, more characterization about the incorporation of the lithium and related to the samples' thicknesses are necessaries to better understand how this dopant can influence the cuprous oxide formation and thus the connected electrical and optical properties.

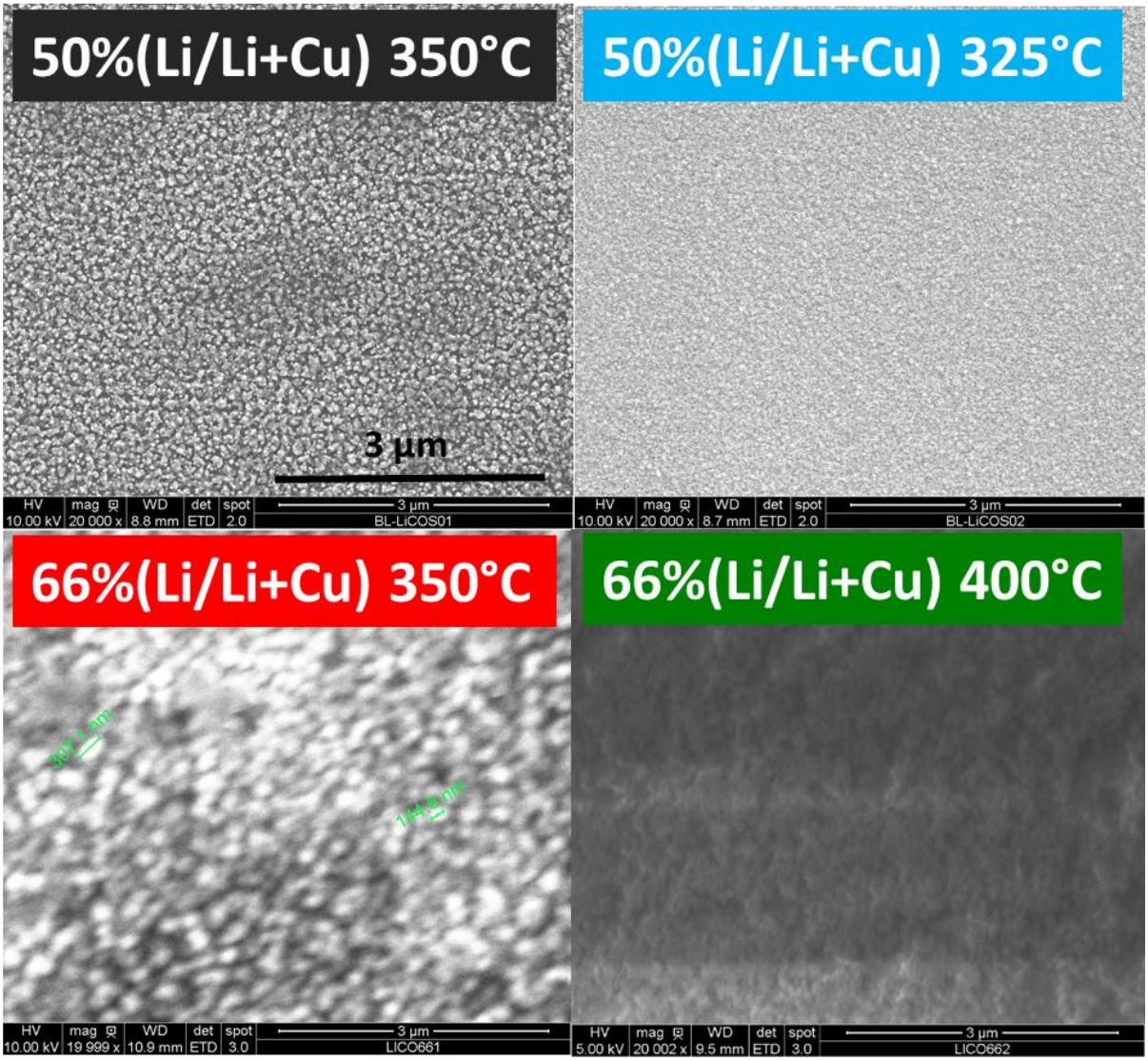

Figure 5.3 SEM images of the surface of the lithium doped copper oxide. In this case, 20000X was used as magnification.

For the 350°C deposition cases, it is possible to see how the amount of lithium strongly modify the surface of the samples. In these two cases, a higher concentration of dopant in the initial solution produces a surface with bigger grains evidenced by the fact that these SEM image were obtained with the same magnification level.

A comparison between the 50%(Li/Li+Cu) cases show that the most uniform surface is obtained when a deposition temperature of 325°C is used. In this case, the roughness is limited; the grains are in contact despite the case where 350°C was used as deposition temperature.

In the case of a higher deposition temperature, a not complete deposition occurred showing a spherical shaped nanoparticle with around 60nm diameter.

For the 66%(Li/Li+Cu) deposited at 350°C, the obtained samples have a spherical nanoparticle with an average diameter of 170nm, which are not connected between them. For the higher

temperature instead, it is noticeable the beginning of the growth of a more uniform film leading to this island shaped film and that generally shows a low roughness.

5.3 Electrical properties

The study of the electrical properties is been performed through the 4-probe measurement and in figure 5.4, it is possible to see the sheet resistance values for each percentage of lithium precursor in the solution for the different deposition temperatures. As reminder it is good to keep in mind that this measurement are the average of the probing in five different points, the edges and the centre of these samples, and the estimated thicknesses of the samples was set to 100nm.

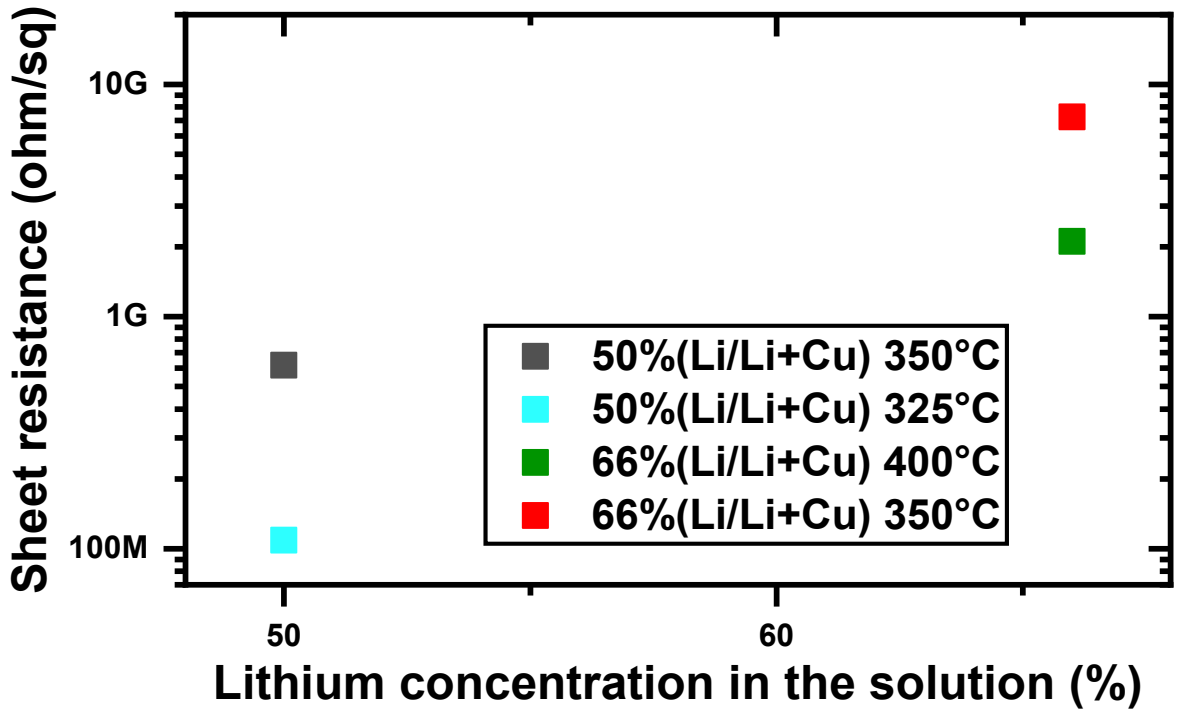

Figure 5.4 Sheet resistance values for lithium doped copper oxide for different deposition temperature

As it is clearly shown from this graph, the case of 50%(Li/Li+Cu) has a decreased sheet resistance when a reduced deposition temperature is used, with a difference between them of around one order of magnitude. In the 66%(Li/Li+Cu) case instead, it is noticeable than a higher deposition temperature leads a lower sheet resistance values. The increment of conductivity in both the cases can be linked with a more uniform surfaces as shown from the previously presented SEM images.

These very high values of sheet resistance can be related to an extremely low thickness of the samples, indeed, the most conductive one has the highest thickness as proved by the transmittance spectrums.

From these results, a comparison with the intrinsic case and the tin doped copper oxide, where the best obtained values of sheet resistance are around 9MΩ/sq, shows that the lithium as dopant does

not correspond to an enhancement of electrical conductivity. Moreover, these depositions took place with the optimized condition for the pure copper oxide and they could not be the best one for this type of doping.

Furthermore, other measurements through ellipsometry, SEM imaging cross-section, AFM and other characterization tools are required to link these values with their thicknesses. Also others investigations are necessaries to better understand the type of charge carriers responsible of the conduction in these materials.

5.4 Optical properties

Probing the transmittance of these samples, the deposited samples show a quite high transmittance as shown in figure 5.5. From the macroscopic point of view, they show an almost transparent macroscopic aspect. There is a great enhancement of the optical properties due to the doping with the lithium with respect to the intrinsic case and the tin doped one.

In the figure is possible to compare the lithium doped copper oxide with the pure copper oxide deposited with the aside listed temperature and a precursor rate of 0,015mmol/min.

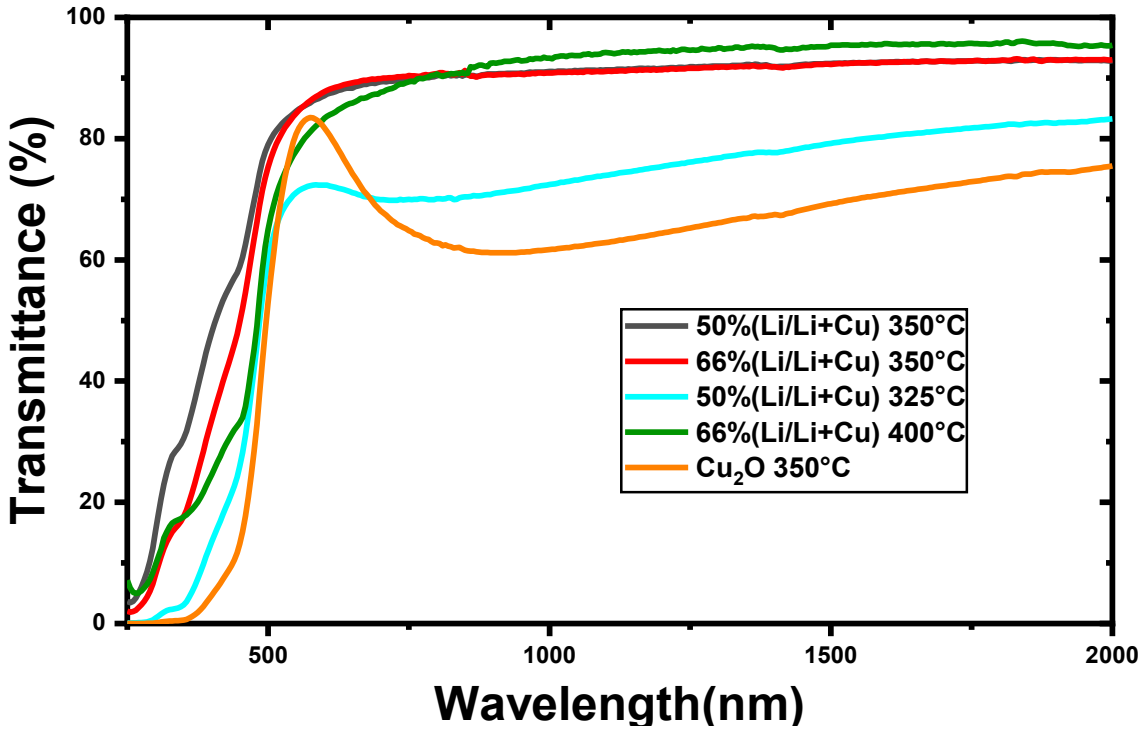

Figure 5.5 Transmittance spectrums of lithium doped copper oxide (Li/Li+Cu) compared with the intrinsic case

As shown here, the transmittance spectrum of 66%(Li/Li+Cu) are very similar except at the beginning of the visible range where a higher deposition temperature leads to a lower transmittance.

For the 50%(Li/Li+Cu) , it is possible to notice that a lower deposition temperature leads to a reduced transmittance and this could be related to the different morphology of the two samples as shown in the paragraph 5.2 as well as the different thicknesses. It is also appreciable that, for the two different level of doping deposited at the same temperature the spectrum is overlapped except at the beginning of the visible range where they slightly differ and a lower level of doping shows an increased transmittance.

According to the high transmittance in IR the deposited samples have a very small thickness. Only for 50%(Li/Li+Cu) deposited at 325°C has a thickness that is closer to pure Cu_2O, around 45nm.

Further studies are necessary to investigate better the optical properties and the thickness effect on them.

It is also possible that due to the lithium presence there is a modification of the energy gap, but no quantification about this parameter were done during this research. For this reason, others analyses should be perform in order to understand the variation of this parameter with the lithium doping.

As last graph, to connect the electrical and optical properties, there is the plot on the average transmittance in the visible range (390nm-700nm) and the sheet resistance values already shown in the previous part.

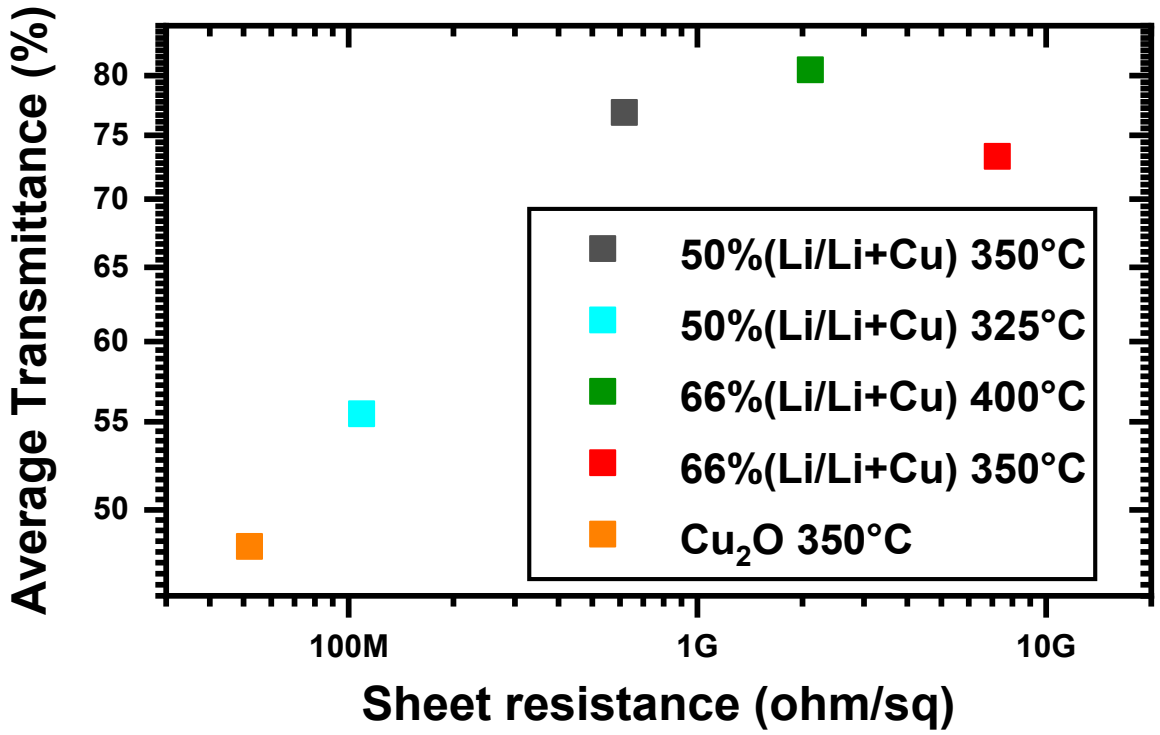

Figure 5.6 Average transmittance plotted with respect to the sheet resistance for lithium doped copper oxide (Li/Li+Cu)

As understandable from the figure 5.6, all the samples present a higher transmittance with respect to the intrinsic case. The highest average transmittance is obtained for the 66%(Li/Li+Cu) case when a deposition temperature of 400°C is used which is the thinnest. The case of 66%(Li/Li+Cu)

shows as the use of an higher deposition temperature increases the average transmittance and reduces the sheet resistance and this difference can be attributed to a different thickness, thus further investigation about the growth of this material are needed.

From the electrical point of view, the 50%(Li/Li+Cu) deposited at 325°C, which is more conductive, is also the one with lowest average transmittance.

These values of sheet resistance are one order of magnitude greater with respect to the case of tin doped cuprous oxide and with respect to intrinsic copper oxide, also.

For the optical properties instead, there is an enhancement with respect to the intrinsic case, reaching values of average transmittance around to 75% when the depositions are performed with a temperature of 350°C or higher.

Conclusions

From the obtained results presented in this work, it is possible to highlight an optimization of the deposition of the intrinsic cuprous oxide. This leads to find a best deposition temperature equal to 325°C, a total molar solution concentration of 0,01mol/l and a solution consumption rate equal to 1,5ml/min i.e. a precursor rate of 0.015mmol/min, obtaining values of sheet resistance around 20 MΩ/sq and average transmittance of 52%. The morphology of the sample shows that these deposition conditions leads to a thickness around 40-50nm with granular structure. The work on this material and its growth through AA-MOCVD process may be further investigate testing different deposition conditions as well as new copper precursors. The thermal annealing affect the sheet resistance values reducing them and this reduction is greater for the samples deposited at 350°C. The calculated activation energies are around 250-300meV, close to the ones reported in literature.

Further researches are required, to better understand the role of the different deposition parameters on the growth and the formation of the crystal and how these are related to the grain structure and to the electrical and optical properties.

In the framework of the different tin precursors effect, many results can be evidenced. The structures are always presenting copper oxide peaks with different intensities based on the precursor. The morphology is similar for all films except for tin (II) acac (liquid) where the film does not cover completely the glass substrate and for tin (II) 2-ethylhexanoate where the films exhibits porous structure with a high roughness.

Moreover, a slight improvement of the conductivity is obtained with the tin doping using tin (II) acetylacetonate (liquid) with values of sheet resistance of 9.1MΩ/sq. The optical properties has been improved through the use of Dibutyltin Diacetate and tin (II) acetylacetonate (liquid) reaching values of average transmittance of 57% and 60%, respectively. Tin (II) 2-ethylhexanoate enhances only the optical properties with a value of average transmittance around 63%.

In all these cases, the EDS analyses show the incorporation of the dopant in the film with different percentages depending on the precursor. As next both the precursors, Dibutyltin Diacetate and tin (II) acetylacetonate (liquid), could be selected for further investigations to understand the role of the tin as dopant and how the different amounts of tin incorporated in the film is connected with the growth of the crystal and the related morphology and structural changes of the layer. Moreover, others studies are necessary to better investigate the oxidation state of tin in the deposited layer and an optimization of the deposition of the doped case could occur. Further thickness studies and measurements on the concentration and nature of the carriers are needed.

Regarding the impact of the different tin dopant levels using the Dibutyltin Diacetate, from the WDS analysis, the depositions successfully incorporate tin, with values close to the 1:1 ratio for concentrations in the solution lower than 30%(Sn/Sn+Cu). This will not strongly modify the structure, as proved by the 30%(Sn/Sn+Cu) case. From the electrical and optical points of view these experiments let conclude that the minimum value is obtained for the 10%(Sn/Sn+Cu) case with sheet resistance value around 20MΩ/sq, as in the intrinsic case, and an enhanced average transmittance of 60%.

Once the incorporation were proved, different questions arise related to the type of semiconducting behaviour, so establishing if the films are p-type or n-type. The role of the incorporation and of the oxidation state in the deposited structure require supplementary investigations, as Hall Effect measurements to understand the charge carriers responsible of the conduction in this material.

For what concern the lithium doped cuprous oxide instead, a resonant phenomenon is evidence by the Raman spectroscopy and this is probably related to photoluminescence defects present in the structures.

From the electrical properties' point of view, the use of this dopant does not imply a reduction of the sheet resistance, with this lithium precursor and with the tested deposition conditions. In fact, the best obtained values in terms of sheet resistance is around 100MΩ, found for the 50%(Li/Li+Cu) case where the lowest deposition temperature was used,325°C.

The use of lithium as dopant, seems to enhance the optical properties of the films with respect to the intrinsic case and to the tin doped one with values of average transmittance greater than 70% when the used deposition temperature is set to 350°C or higher and this occur for both the studied percentage of lithium.

Others characterizations are required to link the optical properties with the thicknesses of the films and to understand how the different deposition conditions change the structural and morphological properties of the samples. Moreover, it would be useful investigate the incorporation and the oxidation state of the lithium in the film to understand how this influence the films' properties.

Others studies should be performed in order to explain how the different amounts of dopant change the properties of the layer. Moreover, the test of different lithium precursors can be analysed in order to have a complete understanding of how these modify the structure and the morphology of the samples.

Bibliography

1. R, J. A. R. Copper-based p-type semiconducting oxides : From materials to devices. (Communauté université Grenoble Alpes, Université De Liege., 2017).
2. Singh, R. & Yadav, B. C. Synthesis and characterization of copper doped tin oxide for humidity sensing applications. *Adv. Sci. Lett.* **20,** 895–902 (2014).
3. Das, S. & Jayaraman, V. SnO2: A comprehensive review on structures and gas sensors. *Prog. Mater. Sci.* **66,** 112–255 (2014).
4. Kuo, C., Huang, C., Chen, J. & Liu, Y. Fabrication of a Miniature Zinc Aluminum Oxide Nanowire Array Gas Sensor and Application for Environmental Monitoring. **2014,** (2014).
5. Drevet, R. *et al.* Metal organic precursor effect on the properties of SnO2thin films deposited by MOCVD technique for electrochemical applications. *Surf. Coatings Technol.* **271,** 234–241 (2015).
6. Priscilla, S. J. *et al.* Structural and Morphological properties of Lithium Doped Copper Oxide Nanoparticles. *Int. J. Mater. Sci.* **12,** 245–249 (2017).
7. Shishiyanu, S. T., Shishiyanu, T. S. & Lupan, O. I. Novel NO2 gas sensor based on cuprous oxide thin films. *Sensors Actuators B Chem.* **113,** 468–476 (2006).
8. Han, G. *et al.* Nitrogen doped cuprous oxide as low cost hole-transporting material for perovskite solar cells. *Scr. Mater.* **153,** 104–108 (2018).
9. Liu, H., Avrutin, V., Izyumskaya, N., Özgür, Ü. & Morkoç, H. Transparent conducting oxides for electrode applications in light emitting and absorbing devices. *Superlattices Microstruct.* **48,** 458–484 (2010).
10. Journal, O. A., Sankarasubramanian, N., Vasuki, R. & Rajathi, S. Effect of Tin as dopant on Zinc Oxide Thinfilms For Solar Cell Applications. **11,** 153–160 (2017).
11. Wang, X., Zhi, L. & Müllen, K. Transparent, conductive graphene electrodes for dye-sensitized solar cells. *Nano Lett.* **8,** 323–327 (2008).
12. Madaria, A. R., Kumar, A. & Zhou, C. Large scale, highly conductive and patterned transparent films of silver nanowires on arbitrary substrates and their application in touch screens. *Nanotechnology* **22,** (2011).
13. Zheng, Q., Li, Z., Yang, J. & Kim, J.-K. Graphene oxide-based transparent conductive films. *Prog. Mater. Sci.* **64,** 200–247 (2014).
14. J. Linnet, A. R. Walther, C. Wolff, O. Albreksten, N. A. Mortensen, J. K.-H. Transparent and conductive electrodes by large-scale nano-structuring of noble metal thin-films. *Opt. Mater. Express* **8,** 1733–1746 (2018).
15. Zhang, Q. *et al.* Copper-doped cobalt oxide electrodes for oxygen evolution reaction prepared by magnetron sputtering. *Int. J. Hydrogen Energy* **37,** 822–830 (2012).
16. Dissertation, a. Thin zinc oxide and cuprous oxide films for photovoltaic applications. *PhD*

Diss. Univ. Minnesota 136 (2010).

17. Hu, F., Zou, Y., Wang, L., Wen, Y. & Xiong, Y. Photostable Cu2O photoelectrodes fabricated by facile Zn-doping electrodeposition. *Int. J. Hydrogen Energy* **41,** 15172–15180 (2016).

18. Lee, Y. S. *et al.* Nitrogen-doped cuprous oxide as a p-type hole-transporting layer in thin-film solar cells. *J. Mater. Chem. A* **1,** 15416–15422 (2013).

19. Kosuke Matsuzaki1, Kenji Nomura2, Hiroshi Yanagi1, Toshio Kamiya1, 2, Masahiro Hirano2, 3, and Hideo Hosono1, 2, 3, A. Epitaxial growth of high mobility Cu2O thin films and application to p-channel thin film transistor. *Appl. Phys. Lett.* (2008).

20. John F.Wager, B. Y. Oxide Thin-Film Transistors: Device Physics. *Semicond. Semimetals* **88,** 283–315 (2013).

21. Minami, T. Present status of transparent conducting oxide thin-film development for Indium-Tin-Oxide (ITO) substitutes. *Thin Solid Films* **516,** 5822–5828 (2008).

22. Presley, R. E. *et al.* Tin oxide transparent thin-film transistors. *J. Phys. D. Appl. Phys.* **37,** 2810–2813 (2004).

23. He, Y., Wang, X., Gao, Y., Hou, Y. & Wan, Q. Oxide-based thin film transistors for flexible electronics. *J. Semicond.* **39,** 011005 (2018).

24. Wang, J. *et al.* Rod-Coating: Towards Large-Area Fabrication of Uniform Reduced Graphene Oxide Films for Flexible Touch Screens. *Adv. Mater.* **24,** 2874–2878

25. Stadler, A. Transparent Conducting Oxides—An Up-To-Date Overview. *Materials (Basel).* **5,** 661–683 (2012).

26. Ellmer, K. Magnetron sputtering of transparent conductive zinc oxide: relation between the sputtering parameters and the electronic properties. *J. Phys. D. Appl. Phys.* **33,** R17–R32 (2000).

27. Jie, L. & Chao, X. XPS examination of tin oxide on float glass surface. *J. Non. Cryst. Solids* **119,** 37–40 (1990).

28. Ellmer, K. Magnetron sputtering of transparent conductive zinc oxide: relation between the sputtering parameters and the electronic properties. *J. Phys. D. Appl. Phys.* **33,** R17 (2000).

29. Nadaud, N., Lequeux, N., Nanot, M., Jovenstitut, J. & Roisnel, T. Structural Studies of Tin-Doped Indium Oxide (ITO) and In 4 Sn 3 O 12. *J. Solid State Chem.* **135,** 140–148 (1998).

30. Losurdo, M. & Bruno, G. Graphene: potential ITO -replacement as transparent conductive layer. *Phys. Chem. Chem. Phys* **13,** (2011).

31. Emmott, C. J. M., Urbina, A. & Nelson, J. Environmental and economic assessment of ITO-free electrodes for organic solar cells. *Sol. Energy Mater. Sol. Cells* **97,** 14–21 (2012).

32. Sato, H., Minami, T., Takata, S. & Yamada, T. Transparent conducting p-type NiO thin films prepared by magnetron sputtering. *Thin Solid Films* **236,** 27–31 (1993).

33. Chen, S. C., Kuo, T. Y., Lin, Y. C. & Lin, H. C. Preparation and properties of p-type

transparent conductive Cu-doped NiO films. *Thin Solid Films* **519,** 4944–4947 (2011).

34. Korzhavyi, P. A. & Johansson, B. Literature review on the properties of cuprous oxide Cu2O and the process of copper oxidation. *Swedish Nucl. Fuel Waste Manag. Co* 8–22 (2011).

35. Duan, N. & Sleight, a W. Transparent p-type conducting CuScO 2 ¿ x films. **77,** 1325–1326 (2000).

36. Huang, D. *et al.* First-principles study of CuAlS2 for p-type transparent conductive materials. *J. Phys. D. Appl. Phys.* **43,** (2010).

37. Biccari, F. Defects and Doping in Cu2O. *Solid State Commun.* 262 (2009). doi:10.1016/0038-1098(70)90325-X

38. Sun, S. *et al.* Cuprous oxide (Cu2O) crystals with tailored architectures: A comprehensive review on synthesis, fundamental properties, functional modifications and applications. *Prog. Mater. Sci.* **96,** 111–173 (2018).

39. Xiang, F.-X., Wang, X.-L. & Dou, S.-X. Transport evidence for the coexistence of the topological surface state and a two-dimensional electron gas in BiSbTe3 topological insulator. *arXiv Prepr.* **1404,** 11 (2014).

40. Georgieva, V., Tanusevski, A. & Georgieva, M. Low Cost Solar Cells Based on Cuprous Oxide. *Sol. Cells–Thin Film …* (1996).

41. Musa, A. O., Akomolafe, T. & Carter, M. J. Production of cuprous oxide, a solar cell material, by thermal oxidation and a study of its physical and electrical properties. *Sol. Energy Mater. Sol. Cells* **51,** 305–316 (1998).

42. Rakhshani, A. E. Preparation, characteristics and photovoltaic properties of cuprous oxide—a review. *Solid. State. Electron.* **29,** 7–17 (1986).

43. Georgieva, V. & Ristov, M. Electrodeposited cuprous oxide on indium tin oxide for solar applications. *Sol. Energy Mater. Sol. Cells* **73,** 67–73 (2002).

44. Nayan, N. *et al.* Sputter Deposition of Cuprous and Cupric Oxide Thin Films Monitored by Optical Emission Spectroscopy for Gas Sensing Applications. *Procedia Chem.* **20,** 124–129 (2016).

45. Jang, J., Chung, S., Kang, H. & Subramanian, V. P-type CuO and Cu2O transistors derived from a sol–gel copper (II) acetate monohydrate precursor. *Thin Solid Films* **600,** 157–161 (2016).

46. Halin, D. S. C., Talib, I. A., Daud, A. R. & Hamid, M. A. A. Characterizations of Cuprous Oxide Thin Films Prepared by Sol-Gel Spin Coating Technique with Different Additives. **2014,** 1141–1145 (2014).

47. H.Kawazoe, K. U. Transparent conductive CuCrO2 thin films deposited by Pulsed Injection Metal Organic Chemical Vapor Deposition: up-scalable process technology for an improved transparency/conductivity trade-off. *Mater. Chem.* (2016).

48. Isseroff, L. Y. & Carter, E. A. Electronic Structure of Pure and Doped Cuprous Oxide with

Copper Vacancies : Suppression of Trap States Electronic Structure of Pure and Doped Cuprous Oxide with Copper Vacancies : (2013). doi:10.1021/cm3040278

49. Nolan, M. & Elliott, S. D. Tuning the Transparency of Cu2O with Substitutional Cation Doping. *Chem. Mater.* **20,** 5522–5531 (2008).

50. Ye, F. *et al.* Doping cuprous oxide with fluorine and its band gap narrowing. *J. Alloys Compd.* **721,** 64–69 (2017).

51. Resende, J., Jiménez, C., Nguyen, N. D., Deschanvres, J. L. & Cu, R. C.-. Magnesium-doped Cuprous Oxide (Mg : Cu 2 O) thin films as a transparent p-type semiconductor oxide. *Phys. Status Solidi* **A,** 2296–2302 (2016).

52. Stéphane Brochen, Laurent Bergerot, Wilfried Favre, João Resende, Carmen Jiménez, Jean-Luc Deschanvres, and V. C. Effect of Strontium Incorporation on the p-Type Conductivity of Cu2O Thin Films Deposited by Metal–Organic Chemical Vapor Deposition. *J. Phys. Chem.* **C,** 17261–17267 (2016).

53. Tsur, Y. & Riess, I. Electrical conductivity of Co doped cuprous oxide. *Ionics (Kiel).* **1,** 488–490 (1995).

54. Sberna, P. M. *et al.* Sputtered cuprous oxide thin films and nitrogen doping by ion implantation. *Thin Solid Films* **600,** 71–75 (2016).

55. Das, S. & Alford, T. L. Structural and optical properties of Ag-doped copper oxide thin films on polyethylene napthalate substrate prepared by low temperature microwave annealing. *J. Appl. Phys.* **113,** (2013).

56. Brandt, I. S. *et al.* Defects controlling electrical and optical properties of electrodeposited Bi doped Cu2O. *J. Appl. Phys.* **123,** (2018).

57. Sieberer, M., Redinger, J. & Mohn, P. Electronic and magnetic structure of cuprous oxide Cu2O doped with Mn, Fe, Co, and Ni: A density-functional theory study. *Phys. Rev. B* **75,** (2007).

58. Chang, Y. Organometallic chemical vapor deposition of copper oxide thin films. (Iowa state university, 1992).

59. Chang, Y.-N. Copper Films Prepared by Metal Organic Chemical Vapor Deposition (MOCVD) Process Using Copper (Acetylacetonate) and Water Vapor as Reactants: The Impact of Water Vapor.

60. Tech, G. Thin Film Deposition and Epitaxy (Chemical Vapor Deposition , Metal Organic CVD and Molecular Beam Epitaxy) Reading : Chapters 13 and 14 Chemical Vapor Deposition. *Chem. Vap. Depos.*

61. Fanciulli, M. G. S. *Rare Earth Oxide Thin Films*. **111,** (Springer US, 2007).

62. Moon, O. M., Kang, B. C., Lee, S. B. & Boo, J. H. Temperature effect on structural properties of boron oxide thin films deposited by MOCVD method. *Thin Solid Films* **464–465,** 164–169 (2004).

63. Wright, P. J. *et al.* Metal organic chemical vapor deposition (MOCVD) of oxides and

ferroelectric materials. **3,** 671–672

64. Song, H. ., Wang, H. ., Zha, S. ., Peng, D. . & Meng, G. . Aerosol-assisted MOCVD growth of Gd2O3-doped CeO2 thin SOFC electrolyte film on anode substrate. *Solid State Ionics* **156,** 249–254 (2003).

65. Xiong, L. *et al.* p-Type and n-type Cu2O semiconductor thin films: Controllable preparation by simple solvothermal method and photoelectrochemical properties. *Electrochim. Acta* **56,** 2735–2739 (2011).

66. Levitskii, V. S. *et al.* Raman spectroscopy of copper oxide films deposited by reactive magnetron sputtering. *Tech. Phys. Lett.* **41,** 1094–1096 (2015).

67. Elfadill, N. G., Hashim, M. R., Chahrour, K. M., Qaeed, M. A. & Wang, C. The influence of oxygen pressure on the growth of CuO nanostructures prepared by RF reactive magnetron sputtering. *J. Mater. Sci. Mater. Electron.* **25,** 262–266 (2014).

68. Nasibulin, A. G., Shurygina, L. I. & Kauppinen, E. I. Synthesis of Nanoparticles Using Vapor-Phase Decomposition of Copper (II) Acetylacetonate. *Coloid J.* **67,** 1–20 (2005).

69. Nasibulin, A. G., Kauppinen, E. I., Brown, D. P. & Jokiniemi, J. K. Nanoparticle Formation via Copper (II) Acetylacetonate Vapor Decomposition in the Presence of Hydrogen and Water - The Journal of Physical Chemistry B (ACS Publications). *J. Phys. Chem. B* 11067–11075 (2001). doi:10.1021/jp0114135

70. Kenvin, J. C. & White, M. G. Selective chemisorption and oxidation/reduction kinetics of supported copper oxide catalysts prepared from copper(II) acetylacetonate. *J. Catal.* **130,** 447–458 (1991).

71. Taylor, J. C. W. & Weichman, F. L. Raman Effect in Cuprous Oxide Compared with Infrared Absorption. *Can. J. Phys.* **49,** 601–605 (1971).

72. Dawson, P., Hargreave, M. M. & Wilkinson, G. R. The dielectric and lattice vibrational spectrum of cuprous oxide. *J. Phys. Chem. Solids* **34,** 2201–2208 (1973).

73. Sander, T. *et al.* Correlation of intrinsic point defects and the Raman modes of cuprous oxide. *Phys. Rev. B* **90,** 45203 (2014).

74. G.Bruhat. *Cours de physique génèrale:Optique*. (Massons et cie, 1965).

75. Deuermeier, J. *et al.* Highly conductive grain boundaries in copper oxide thin films. *J. Appl. Phys.* **119,** (2016).

76. Berthomieu, B. & Menasche, M. An enumerative approach for analyzing time Petri nets. *Proceedings IFIP* 41–46 (1983). doi:10.1007/3-540-45014-9

77. Siripala, W., Perera, L. D. R. D., De Silva, K. T. L., Jayanetti, J. K. D. S. & Dharmadasa, I. M. Study of annealing effects of cuprous oxide grown by electrodeposition technique. *Sol. Energy Mater. Sol. Cells* **44,** 251–260 (1996).

78. Akgul, F. A., Akgul, G., Yildirim, N., Unalan, H. E. & Turan, R. Influence of thermal annealing on microstructural, morphological, optical properties and surface electronic structure of copper oxide thin films. *Mater. Chem. Phys.* **147,** 987–995 (2014).

79. Nerle, U. Thermal Oxidation of Copper for Favorable Formation of Cupric Oxide (CuO) Semiconductor. *IOSR J. Appl. Phys.* **5,** 01–07 (2013).

80. Suh, S. *et al.* Precursor Oxidation State Control of Film Stoichiometry in the Metal−Organic Chemical Vapor Deposition of Tin Oxide Thin Films. *Chem. Mater.* **9,** 730–735 (1997).

81. Kavitha, K., Rao, T. S. & Suvarna, P. Analysis of the Properties of Cu Doped Tin Oxide and Tin Doped CuO Thin Films. 1795–1796 (2016).

82. Vomáčka, P., Štengl, V., Henych, J. & Kormunda, M. Shape-controlled synthesis of Sn-doped CuO nanoparticles for catalytic degradation of Rhodamine B. *J. Colloid Interface Sci.* **481,** 28–38 (2016).

83. Tripathy, S., Nagarjun, B. & Jahnavy, V. Optical and Structural Characteristics of Copper Doped Tin Oxide Thin Film Prepared by Thermal Evaporation Method. *Int. J. Eng. Innov. Technol.* **3,** 296–300 (2013).

84. Sakthiraj, K., Karthikeyan, B. & Balachandrakumar, K. Structural , Optical and Magnetic properties of Copper (Cu) doped Tin oxide (SnO 2) nanocrystal. **7,** 1481–1487 (2015).

85. Roy, S. S. & Podder, J. Studies on tin oxide (SnO2) and Cu doped SnO2 thin film deposited by spray pyrolysis technique for window material in solar. *Proc. Int. Conf. Mech. Eng.* **2009,** 26–28 (2009).

86. Melsheimer, J. & Ziegler, D. Thin tin oxide films of low conductivity prepared by chemical vapour deposition. *Thin Solid Films* **109,** 71–83 (1983).

87. Fan, W. *et al.* Facile Synthesis and Optical Property of Porous Tin Oxide and Europium-Doped Tin Oxide Nanorods through Thermal Decomposition of the Organotin. *J. Phys. Chem. C* **112,** 19939–19944 (2008).

88. Sberveglieri, G. *et al.* Enhanced response to methane for SnO2 thin films prepared with the VCD technique. *Sensors Actuators B Chem.* **16,** 334–337 (1993).

89. Mannie, G. J. A. & Niemantsverdriet, P. D. J. W. Surface chemistry and morphology of tin oxide thin films grown by chemical vapor deposition. 1–177 (2013). doi:10.6100/IR751861

90. Ashida, T. *et al.* Thermal transport properties of polycrystalline tin-doped indium oxide films. *J. Appl. Phys.* **105,** (2009).

91. Srinivasa Murty, N. & Jawalekar, S. R. Characterization of antimony-doped tin oxide films for solar cell applications. *Thin Solid Films* **108,** 277–283 (1983).

92. Mohd Hanif, A. S., Lau, W. K., Mohamad, F., Wan Zaki, W. S. & Ahmad, M. K. Preparation of Nanostructured Fluorine Doped Tin Oxide (FTO) by Hydrothermal Method. *Appl. Mech. Mater.* **773–774,** 632–636 (2015).

93. Tadeev, A. ., Delabouglise, G. & Labeau, M. Sensor properties of Pt doped SnO2 thin films for detecting CO. *Thin Solid Films* **337,** 163–165 (1999).

94. Canevali, C. *et al.* Substitutional tin-doped silica glasses: an infrared study of the sol–gel transition. *J. Non. Cryst. Solids* **293–295,** 32–38 (2001).

95. Norberto Chiodini, Franco Meinardi, Franca Morazzoni, Jin Padovani, Alberto Paleari, R. S. and G. S. Thermally induced segregation of SnO2 nanoclusters in Sn-doped silica glasses from oversaturated Sn-doped silica xerogels. *J. Mater. Chem.* **11,** 926–929 (2001).

96. Pabchanda, P. M. ; S. Influence of Tin Doping on the Photocatalytic Activity of Zinc Oxide Thin Films under UV Light. *J. Chem. Chem. Eng.* **6,** 631–637 (2012).

97. Yim, K. Computational discovery of p-type transparent oxide semiconductors using hydrogen descriptor. *npj Comput. Mater.* (2018). doi:10.1038/s41524-018-0073-z

98. Saito, K. *et al.* Phase diagram of lithium-doped copper oxide, Cu1-xLixO. *Solid State Commun.* **125,** 23–26 (2003).

99. Tae Gyoum Kim, Hyukhyun Ryu, W.-J. L. Effects of lithium (Li) on lithium-cuprous-oxide (Li-Cu2O) composite films grown by using electrochemical deposition for a PEC photoelectrode. *J. Korean Phys. Soc.* 268–273 (2016).

100. Peng, N. *et al.* Effect of lithium-site doping on enhancing the lithium storage performance of SrLi2Ti6O14. *Electrochim. Acta* **265,** 437–447 (2018).

101. Park, M. S. *et al.* A novel lithium-doping approach for an advanced lithium ion capacitor. *Adv. Energy Mater.* **1,** 1002–1006 (2011).

102. Han, S. S. & Goddard, W. A. Lithium-Doped Metal-Organic Frameworks for Reversible H 2 Storage at Ambient Temperature. *J. Am. Chem. Soc.* **129,** 8422–8423 (2007).

103. Rai, V. K., Rai, D. K. & Rai, S. B. Pr3+ doped lithium tellurite glass as a temperature sensor. *Sensors Actuators A Phys.* **128,** 14–17 (2006).

104. Iijima, T., Toyoguchi, Y., Nishimura, J. & Ogawa, H. Button-type lithium battery using copper oxide as a cathode. *J. Power Sources* **5,** 99–109 (1980).

105. Thi, T. V., Rai, A. K., Gim, J. & Kim, J. Potassium-doped copper oxide nanoparticles synthesized by a solvothermal method as an anode material for high-performance lithium ion secondary battery. *Appl. Surf. Sci.* **305,** 617–625 (2014).

106. Félix del Prado, Ana Cremades, Julio Ramírez-Castellanos, David Maestre, J. M. G.-C. and J. P. Effect of lithium doping and precursors on the microstructural, surface electronic and luminescence properties of single crystalline microtubular tin oxide structures. *CrystEngComm* (2017).

107. Garduño, I. A. *et al.* Optical and electrical properties of lithium doped nickel oxide films deposited by spray pyrolysis onto alumina substrates. *J. Cryst. Growth* **312,** 3276–3281 (2010).

108. Sebagai, K. L., Keatas, P., Serbuk, M. & Magnesium, N. Effects of Lithium Dopant on Size and Morphology of Magnesium Oxide Nanopowders. **18,** 15–20 (2014).

109. Chang, Y.-T. *et al.* Excellent piezoelectric and electrical properties of lithium-doped ZnO nanowires for nanogenerator applications. *Nano Energy* **8,** 291–296 (2014).

110. Giordano, F. *et al.* Enhanced electronic properties in mesoporous TiO2 via lithium doping for high-efficiency perovskite solar cells. *Nat. Commun.* **7,** 10379 (2016).

111. Rooksby, H. P. & Vernon, M. W. Lithium- and gallium-doped nickel oxide. *Br. J. Appl. Phys.* **17,** 1227 (1966).

112. Al-Jawhari, H. A., Caraveo-Frescas, J. A., Hedhili, M. N. & Alshareef, H. N. P-Type Cu2O/SnO Bilayer Thin Film Transistors Processed at Low Temperatures. *ACS Appl. Mater. Interfaces* **5,** 9615–9619 (2013).